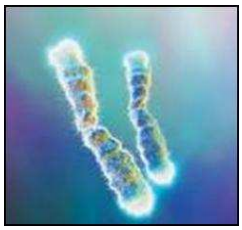

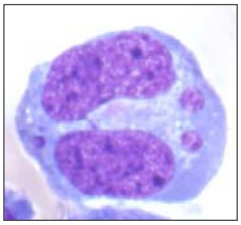

The impact of folate on telomere length and chromosome stability in human WIL2-NS cells and lymphocytes

Caroline Felicity Bull

November 2009

THE UNIVERSITY OF ADELAIDE
AUSTRALIA

SUB CRUCE LUMEN

CSIRO

CHAPTER 1: INTRODUCTION

1 INTRODUCTION

1.1 CHROMOSOME INSTABILITY, GENOME DAMAGE AND DISEASE

Chromosome instability and genome damage is a key initiating factor in numerous conditions including cancers[1,2], infertility[3], neurodegenerative diseases[4,5] and accelerated ageing syndromes[6,7]. Large prospective studies conducted over several countries demonstrated that increased chromosomal aberrations in peripheral blood lymphocytes (PBL) is a predictor of future cancer risk[8-11]. These studies investigated the incidence of chromosome-type aberrations (CSAs) and chromatid-type aberrations (CTAs) and they focussed specifically on cancer risk, while correcting for exposure to potential carcinogens such as smoking or workplace hazards[8,9]. Results suggested that both DNA double-strand breaks and other initial DNA lesions responsible for CSAs and CTAs were associated with cancer risk[10].

DNA is continuously under threat of major mutations by a variety of mechanisms. These include point mutation; base modification due to reactive molecules such as the hydroxyl radical; chromosome breakage and rearrangements; chromosome loss or gain; silencing of housekeeping genes or expression of parasitic DNA due to aberrant methylation of CpG islands in gene promoter regions; and accelerated telomere shortening or dysfunction[12,13]. There are many assays for determining DNA damage, such as the identification of aneuploidy, DNA adducts or oxidation, and DNA strand breaks[12]. One of the most widely used is the CBMN Cytome assay, which has been developed into a comprehensive system for measuring DNA damage and misrepair, chromosomal instability, mitotic abnormalities, cell death, and cytostasis[14].

1.1.1 Determination of chromosomal damage using the CBMN Cytome assay

Developed originally as a marker of radiation exposure and damage, the CBMN assay has evolved into the CBMN Cytome Assay. This assay is widely recognised as a sensitive and precise means of quantifying genome instability and chromosome damage due to ageing, dietary and lifestyle factors, or exposure to carcinogens. It involves culturing lymphocytes from a blood sample, blocking cells at cytokinesis using cytochalasin-B (Cyto-B), and identifying once divided cells by their binucleate appearance for the purpose of scoring damage biomarkers via light microscopy[14]. Cytostasis effects are measured by the proportion of mono-, bi-, or multinucleated cells, and cytotoxicity via the frequencies of necrotic and/or apoptotic cells[14]. While it was developed initially to measure chromosomal damage by scoring micronuclei (MNi), the assay now also incorporates scoring of nuclear buds (NBuds) and

nucleoplasmic bridges (NPBs) (also known as anaphase bridges) as validated biomarkers of genome damage (Figure 1.1)[14].

1.1.1.1 Micronuclei

MNi originate from chromosome fragments or whole chromosomes that lag behind at anaphase during nuclear division[14]. These can arise from malsegregation of chromosomes due to spindle or kinetochore defects or from cell-cycle checkpoint malfunction, unrepaired chromosome breaks, DNA misrepair, acentric chromosome fragments and/or asymmetrical chromosome rearrangement[14]. MNi can also occur in cells containing NPBs and/or NBuds. Frequency of MNi has been shown to increase with ageing, with dietary micronutrient insufficiencies and with exposure to clastogenic and aneugenic agents[15]. The Human Micronucleus (HUMN) international collaborative project involved 20 laboratories in 10 countries, following 6718 subjects over 22 years, in order to validate MN frequency for use as a biomarker of chromosomal damage and genome stability in humans[16]. Findings from this study demonstrated that participants with a medium or high frequency of MNi had a significant increase in cancer incidence, as well as decreased cancer-free survival. These data provided preliminary evidence that MN frequency in PBL had value as a predictive biomarker of cancer risk within a population of healthy subjects[16]. Further long term studies conducted over 14 years have confirmed these initial findings; demonstrating frequency of MNi in PBL of disease-free subjects to be a strong predictor for risk of death from cancer or from cardiovascular disease (CVD)[17,18].

1.1.1.2 Nuclear Buds

Aberrations in copy number of genomic DNA is frequently seen in solid tumours, and is believed to contribute to the evolution of the tumour[19]. Amplification events can result in net gain or loss of whole chromosomes (leading to aneuploidy), or parts of chromosomes[19]. First reported in 1984, drug-resistant cell lines were found to permit gene amplification, while normal cells were protected by preventive mechanisms, such as checkpoint controls[19,20]. Miele *et al* (1989) demonstrated in Chinese hamster cells that resistance to cytotoxic drugs, such as methotrexate, was mediated by gene amplification and gave rise to bud-shaped formations in interphase nuclei which would later separated to form MNi[21]. Amplification-bearing dicentric chromosomes were also found in drug-resistant cell lines[21]. Approximately 50% of the resultant NPBs underwent asymmetric breakage, giving rise to chromosomes with varied gene copy numbers[21]. Taken together, the evidence indicated to these researchers that the presence of an amplified region of DNA rendered the chromosome unstable and more susceptible to rearrangements than normal chromosomes[21]. Later research by Shimizu *et al* showed that

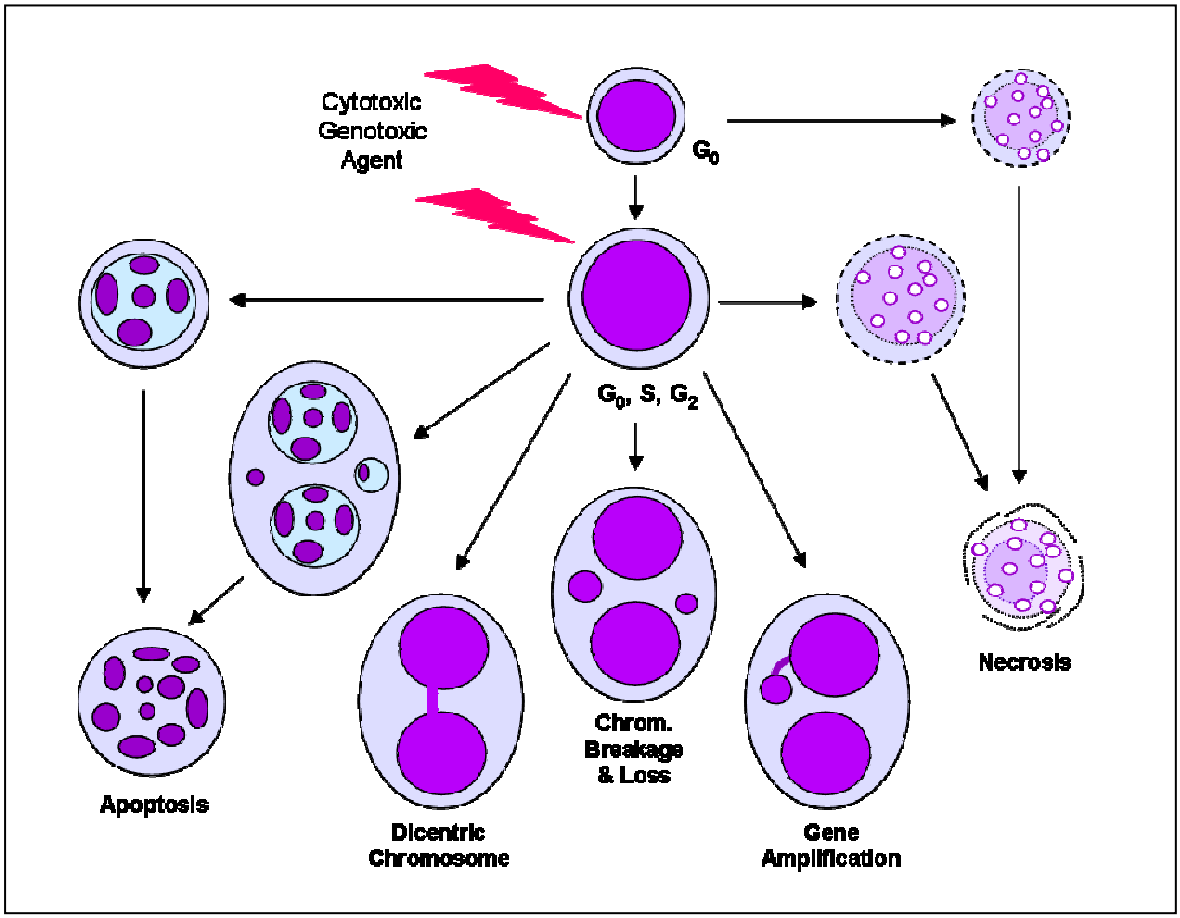

Figure 1.1 The various possible fates of cultured cells in which cytokinesis was blocked following exposure to cytotoxic/genotoxic agents. Using the morphological biomarkers that can be observed by microscopy in the Cytokinesis-block Micronucleus Cytome (CBMN-Cyt) assay, it is possible to measure: the frequency of nucleoplasmic bridges (NPB), a biomarker of asymmetrical chromosome rearrange-ments that result in dicentric chromosomes due to mis-repair of chromosome breaks or telomere end fusions; micronuclei (MNi), a biomarker of chromosome breakage or loss; nuclear buds (NBuds), a biomarker of gene amplification; apoptosis and necrosis. (Adapted from Fenech *et al*, 2003[22,23]).

amplified DNA is selectively localised to specific sites at the periphery of the nucleus, where it can be eliminated via nuclear budding (NBuds) to form MNi during S phase of mitosis[24,25]. The mechanism for NBud formation is believed to involve recombination between homologous regions within amplified sequences, leading to formation of mini-circles of acentric and atelomeric DNA (double minutes)[14]. Double minutes are small circular fragments of extrachromosomal DNA, up to a few million base pairs in size, possibly conferring a selective advantage for the cell[26]. DNA of double minutes can, under some circumstances, reintegrate at other sites in chromosomes, leading to further chromosomal instability (CIN)[27]. In some cases, the amplified DNA is formed by a complex process that involves multiple chromosomes[19]. NBuds are characterised by having the same morphology as MNi, with the exception that they are linked to the nucleus by either a narrow or wide stalk of nucleoplasmic material, depending on the stage of the budding process[14]. The process for extrusion of the excess DNA from the cell is unknown at this stage[14]. Studies correlating NBuds with MNi in lymphocytes provided evidence that NBuds are a valid biomarker for inclusion in the standard CBMN Cytome assay, and that they are reliable markers of genome instability[28]. For example, in a recent study MNi, NBuds and NPBs were all shown to be strong predictors of lung cancer risk, with 25% of lung cancer patients (versus just 5% of controls) having ≥1 spontaneous NBud in mitogen stimulated lymphocytes. This calculated to equate with a 6-fold increase in cancer risk[29].

1.1.1.3 Nucleoplasmic bridges

NPBs are a marker of dicentric chromosomes and they are thought to result either from mis-repair of DNA at a double strand break (DSB) or from end-fusions of chromosomes arising from dysfunctional telomeres[14]. They occur when the centromeres of dicentric chromosomes are pulled to opposite poles of the cell at anaphase[14]. NPBs are not visualised under normal conditions of cell division, because they are broken at telophase. However, when cell division is blocked at the binucleate stage with Cyto-B, NPBs remain unbroken and they become enveloped by nuclear membrane. Under these conditions, they are clearly visible by light microscopy[14]. NPBs and MNi are regularly observed in the same cell, indicating that chromosomal fusion arising from a double strand break has occurred, forming both a dicentric chromosome and an acentric fragment[14,30]. As explained by Thomas *et al* from observations in both WIL2-NS cells and lymphocytes, the location and frequency of DSBs within a chromatid, the point in the cell cycle at which breakage occurs, and the stage at which repair is undertaken are all factors which potentially alter the incidence of NPBs within binucleated cells[30]. NPBs may occasionally contain DNA from more than one (non-homologous) chromosome, but often they contain DNA from a single chromosome[30]. Telomere dysfunction is strongly implicated

in the formation of chromosome end fusions and this is discussed in greater detail (Chapter 1.3.6 below). A strong dose dependent correlation has been observed between NPBs and MNi in cells exposed *in vitro* to reactive oxygen species, γ-radiation and micronutrient deficiency[28,30].

1.1.1.4 Breakage-fusion-bridge cycles

The formation of NPBs is a key initiating factor in the breakage-fusion-bridge (BFB) cycle[27]. As stated above, a dicentric chromosome is formed either from mis-repair of a DSB, or from the fusion of dysfunctional chromosome ends (telomeres). Once formed, a dicentric chromosome is unable to successfully separate at anaphase, thus forming a DNA bridge between the two poles prior to telophase. At mitosis, the mechanical stress on the NPB causes asymmetrical breakage, resulting in an uneven gene allocation to each daughter cells. The presence of these broken unprotected chromosomes in the daughter cells forms the focus of further DNA repair processes, with a high likelihood of generating further dicentric chromosomes. These are then replicated, thus amplifying and repeating the cycle[19,28,30] (Figure 1.2). By this process of recombination of damaged chromosomes, the BFB cycle has been shown to instigate ever-increasing levels of genomic disarray and instability, and has been strongly associated with early changes in cancers[12,31,32]. BFB cycling provides a means by which a cell can amplify genes that could, by chance, confer selective advantage against a stressful environment (*eg.* micronutrient deficiency, exposure to carcinogens or cytotoxic drugs), increase the capacity for proliferation, allow a DNA checkpoint to be circumvented and/or promote evasion of immune responses[12,33].

In vitro studies have demonstrated that BFB cycles can last for many cell generations after the initial insult has been removed[33], but can be resolved by addition of a new telomere to exposed chromosome ends[27]. The latter may result from non-reciprocal transfer, or duplication, of all or part of an arm of another chromosome[27]. However, non-reciprocal transfer results in the donor chromosome itself becoming uncapped and unstable[27]. As an example, osteosarcoma is characterised by chromosomal instability and high copy number gene amplification[31]. Studies using OS cells lines showed each had increased levels of NPB, dicentric chromosomes, and instability of both chromosome structure and chromosome number[31]. Another study in lung cancer cells demonstrated that alterations in copy number of chromosome 7 in lines that were resistant to the drug paclitaxel originated from repeated BFB cycles[32]. *In vitro* studies using WIL2-NS cells and peripheral blood lymphocytes (PBL) grown in folate-deficient medium have also consistently shown increases in MNi, NBuds and NPBs, all three of which are biomarkers of genomic instability. The latter suggests of a model in which BFB cycling results

in the sort of hypermutable phenotype that is required for the rapid evolution of cancer cells[14,28,30].

1.2 MICRONUTRIENTS AND CHROMOSOME INSTABILITY

Recommended dietary intakes (RDIs) have been established for a broad list of essential vitamins, minerals and trace elements. They specify the small daily amounts of these nutrients that are believed necessary to maintain normal health in a given population[34]. A deficiency, on the other hand, is defined as a level of daily intake that is 50% or less of these RDI values. Acute deficiencies, such as scurvy arising from vitamin C deficiency, are rare in developed countries. Nevertheless, many individuals consume a diet that falls short of the recommended intakes of essential nutrients. Review of evidence has shown that insufficiencies in a number of micronutrients, including iron, zinc, folate, vitamins B12, vitamin B6 and vitamin C, can lead to DNA damage, genomic instability and the potential for cancer development[34].

Results from a recent population study suggest that at least nine micronutrients affect genome stability[35]. These findings are from a cytogenetic epidemiological study on 190 healthy individuals (mean age 47.8 years, 46% males) designed to determine whether there was an association between diet (and thus dietary intake of micronutrients), measured using a food frequency questionnaire combined with an analysis of genome damage in lymphocytes, measured using the CBMN assay[35]. Multivariate analysis of base-line data showed that (a) in a comparison between individuals in the highest and lowest tertiles of intake of vitamin E, retinol, folate, nicotinic acid (preformed) and calcium, there was a significant reduction in MN frequency (-28%, -31%, -33%, -46%, and -49% respectively), in those in the highest tertile group (b) the highest tertile of intake of riboflavin, pantothenic acid and biotin was associated with significant increases in MN frequency (+36%, +51% and +65%, respectively) relative to lowest tertile of intake[35]. Mid-tertile β-carotene intake was associated with an 18% reduction in MN frequency relative to the lowest tertile, but the highest tertile of intake (>6400μg/d) had an 18% increment in MN frequency over the lowest tertile group[35]. The results from this study illustrate that a wide variety of micronutrients have a strong impact on genome health, depending on level of intake. The amounts of micronutrients that appear to be protective against genome damage vary greatly between foods and careful choice is needed to design dietary patterns that are optimised for maintenance of genome health[1].

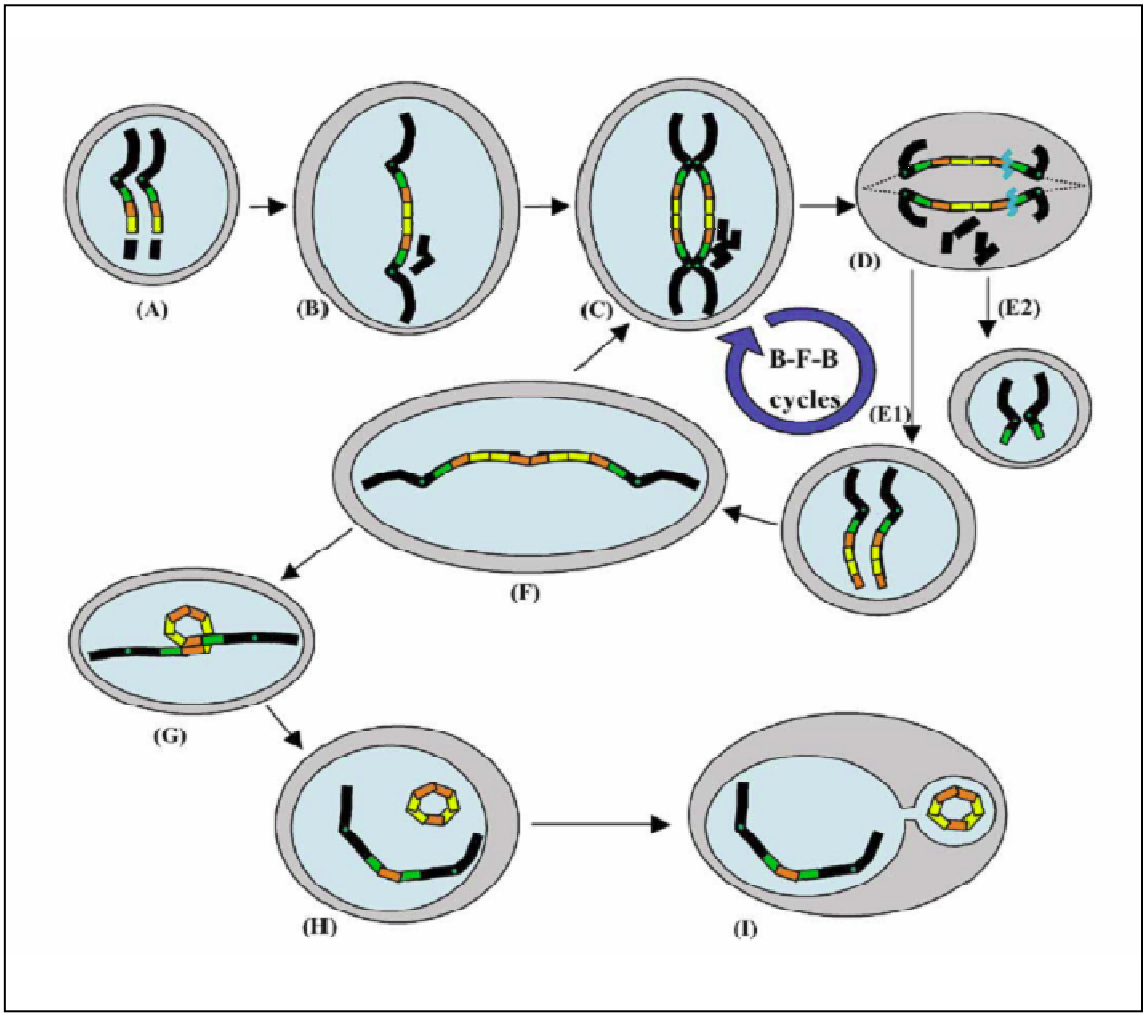

Figure 1.2 Gene amplification by breakage-fusion-bridge (BFB) cycles

Broken sister chromatids (A) fuse at the 'sticky' ends to form a dicentric chromosome (B). The dicentric chromosome is replicated in S phase (C), and the centromeres may then be drawn to opposite poles during anaphase resulting in the formation of a nucleoplasmic bridge (D). In this example, the dicentric chromosome breaks in a non-central region resulting in one daughter cell receiving chromosomes that contain two copies of the yellow and red genes (E1), while these genes are deleted in the corresponding chromosomes of the other daughter cell (E2). The chromosomes with multiple copy number may fuse again (F) to propagate the amplification cycle (back to step C). Alternatively, recombination may occur between homologous sequences (G) and result in the 'looping-out' of a circular acentric DNA fragment, or double minute, (H) which is subsequently extruded from the nucleus via budding (I) (Adapted from Fenech & Crott, 2002[28]).

1.2.1 Folate insufficiency and disease risk

Folate deficiency can occur due to inadequate dietary intake (sometimes associated with high alcohol consumption), certain drug therapies, impaired intestinal absorption (including the effect of high alcohol consumption), impaired renal tubular reabsorption, or altered activity of metabolic enzymes due to genotype[36-39]. Deficiency of this micronutrient has been shown to have deleterious health effects, with implications for increased risk of neural tube defects (NTDs), anemia, neurodegenerative diseases[40] and development of cancer[34,38]. Dietary intake of folate correlates inversely with risk of developing colorectal cancer, and has been shown to be protective in high-risk patients with chronic ulcerative colitis[41]. Similarly, low folate status has been associated with pancreatic cancer in smokers[42], and with increased risk of oesophageal and gastric cancers[43]. There is also suggestion that low folate status, leading to high plasma homocysteine (Hcy) concentrations, may be a risk factor in Alzheimer's disease and some other neurodegenerative conditions[44]. There is contradictory evidence in relation to whether folate and other B group vitamins have a role in protection against breast cancer in women, particularly with respect to intake of alcohol and its effects on folate absorption[34,36,38]. Several studies have shown that lower folate status is associated with an increased risk of breast cancer[45-47], while other large retrospective studies on vitamin intake and cancer outcome have been inconclusive[48,49]. Prenatal consumption of folate has been proposed to have a protective effect for childhood cancers, including leukemia[50]. A meta-analysis conducted on consumption of multivitamins during pregnancy suggested that vitamin supplementation reduced the risk of childhood leukemias, neuroblastoma and paediatric brain tumours[51]. Studies specifically focussed on folate consumption have confirmed a protective effect of prenatal folate intake on the incidence of childhood acute lymphoblastic leukemia[39,52,53]. The genetic background of the mother, and her ability to metabolise folate, also appear to be important factors for risk of childhood leukemias[39,52].

1.2.2 Folate: Recommended daily intake (RDI) and fortification of foods

Folate (vitamin B9), a dietary factor known to be critical for maintenance of genome stability; is a water soluble micronutrient that is present in many foods. High levels are found in leafy green vegetables, whole grain foods, legumes, oranges and some meats. The stable synthetic (unreduced, unmethylated, monoglutamated) form used in supplements, is known as 'folic acid' (FA)[54]. As a cofactor required for nucleotide and methionine synthesis and for methylation processes, folate is critical for integrity of DNA replication, the effective functioning of many DNA repair enzymes, and for regulation of gene expression by the methylation state of histones[35,55-57]. Due to the rapid cell division which takes place during embryonic and foetal development, the importance of folate in the prevention of birth defects

has long been recognised. Neural tube defects (NTDs) such as spina bifida, and a range of other non-NTD birth defects (such as cardiac and urinary tract anomalies, orofacial clefts and limb reduction defects) have all been associated with folate insufficiency[58,59]. Furthermore, low plasma folate levels in adults have been associated with increased risk of cardiovascular disease (CVD), stroke and chromosomal instability leading to cancers[60-62]. Such is the importance of folate for dividing cells that anti-folate drugs were developed to halt the growth of tumours. One such example is methotrexate, a drug widely used as a cancer therapeutic to block folate in the dihydrofolate form (DHF). Methotrexate prevents formation of tetrahydrofolate (THF), thus inhibiting the progression of the folate cycle (see below).

The current RDI for folate for adult Australians is 400µg/day, increased by the National Medical Health & Research Council (NHMRC) in 2005 from the previous level of 200µg/day. Mammals lack the ability to synthesise folate *de novo* and require, therefore, preformed folate in the diet. However, large losses of folate can occur during food preparation (*eg.* heating), particularly under oxidative conditions[63]. As a result, it is difficult for individuals to achieve the recommended intake from diet alone. FA, the synthetic form of folate used in supplements, is more bioavailable than the form commonly found in foods. Many nations, including the majority of western countries, now fortify the food supply with FA via grain products, with other countries currently in the process of implementing fortification strategies. The United States of America (USA) and Canada, for example, have had mandatory fortification since 1998, while Australia has implemented this measure as of September 2009. Important comparative studies have been carried out to assess the incidence of birth defects, CVD, stroke and certain cancers in countries with and without mandatory FA fortification in the food supply. A significant reduction in stroke mortality was observed in the USA and Canada in association with increased plasma folate levels and reduced levels of plasma homocysteine (Hcy). Raised levels of Hcy are a known risk factor for CVD and stroke (see below)[64]. A reduction in NTDs has been observed in countries where folate fortification has been implemented, while comparable reductions have not been recorded in countries without supplementation[65]. The data supporting protective effects of FA fortification on non-NTD birth defects is less emphatic compared with that for NTDs, but some modest benefits appear to have been gained in reducing the prevalence of some of these conditions[59].

While the evidence associating low folate status with chromosome instability and disease risk is strong, concerns have been raised regarding the dangers of excessive amounts of folate supplementation. The NHMRC, in the 2006 RDI guidelines, proposed an upper limit of 1000µg/day[66]. It is known that some pre-cancerous cells up-regulate FA receptors, and in

those cases high dose supplementation of FA could encourage division and proliferation of aberrant cells, thus enhancing tumour growth[67,68]. Some researchers believe further study is required to determine healthy upper limits for folate intake, with particular reference to widespread supplementation of FA via the food supply, together with the widespread occurrence of vitamin self-medication in the community[69]. The NHMRC, on the other hand, reported that median folate intakes in the Australian and New Zealand populations are significantly below the RDI of 400µg/day recommended in the 2005 guidelines; at around 320µg/day for men and 230µg/day for women. They also propose that the daily intake of folate required for prevention of cardiovascular and chronic disease, and reduction of DNA damage and related cancer risk, may be as high as 700µg/day[66].

1.2.3 Folate structure, one carbon metabolism and the folate pathway

Folates are a family of compounds that have pteroylglutamic acid (PteGlu) as a common structure (Figure 1.3A)[70]. They differ from each other by pyrazine ring substitutions and by the number of glutamate residues that are added (Figure 1.3A)[70]. Natural folate compounds exist in plasma and urine in a monoglutamate form, 5-methyltetrahydrofolate (5-MeTHF) (Figure 1.3B), which can readily be transported across the cell membrane[71]. 5-MeTHF is polyglutamated within the cell, where it enters the folate cycle (Figure 1.4). 5,10-methyltetrahydrofolate (5,10-MeTHF) is the methyl donor responsible for methylation of dUMP to dTMP (Figure 1.3C). The pyrazine ring may be partially reduced at the 7, 8 positions by dihydrofolate reductase to form dihydrofolate (DHF, $H_2PteGlu_n$) (Figure 1.3D), or fully reduced to tetrahydrofolate (THF, $H_4PteGlu_n$) (Figure 1.3E). The latter, tetrahydrofolate (Figure 1.3E), is the active carrier of one carbon units within the cell[71].

The essential role of folate in cellular processes is that of donating one carbon units (methyl groups) in a number of reactions[71]. This role is effected via two distinct, but interconnected, biochemical pathways: (a) maintenance methylation of cytosine in DNA, which is required to maintain or control gene expression patterns and chromosomal structural integrity; and (b) methylation of dUMP to produce dTTP required for DNA synthesis (Figure 1.4). For DNA methylation, folate donates its methyl group to Hcy to generate methionine and ultimately S-adenosyl methionine (SAM), the universal methyl donor. This reaction, converting Hcy to methionine, is catalysed by methionine synthase (MTR) and requires vitamin B12 as a cofactor[72]. Methylation of DNA is performed by DNA methyltransferase (DNMT) enzymes, which utilise SAM as methyl donor[73].

Another vital role of folate is as a methyl donor for converting dUMP to dTTP. Thus folate has a key role in ensuring the supply of this essential nucleotide for DNA synthesis and DNA repair[74]. Under conditions of low folate, the cell is unable to produce sufficient dTTP, and as a result uracil is incorporated into DNA in place of thymine[74]. Subsequent excision of uracil by glycosylases leaves abasic sites, which are potential sites for strand breaks and thus generation of acentric chromosome fragments and formation of micronuclei[75]. The implications of this effect are discussed in greater detail below (Chapter 1.2.7).

1.2.4 Homocysteine

Homocysteine (Hcy) is a homologue of the amino acid cysteine, differing by the presence of an additional methylene (-CH_2) group that precedes the thiol (-SH) group in the side chain. The compound is formed from S-adenosyl homocysteine, and can then be converted back to methionine by methionine synthase (MTR) with its cofactor, vitamin B12 (Figure 1.4). Hcy and folate have an inverse relationship in plasma, and for this reason plasma Hcy is recognised to be a sensitive metabolic marker of folate and vitamin B12 status and bioavailability[76]. When folate is limiting, the cellular concentration of 5-methyl THF (the substrate for MTR) is reduced, causing plasma Hcy to increase[77]. Elevated plasma Hcy is a known risk factor for cardiovascular disease (CVD)[78,79] and NTDs[80,81]. It has also been implicated in cognitive deficit (in the elderly)[82], bipolar disorder and depression[83,84], and in neurodegenerative states such as Alzheimer's disease[85]. Long term *in vivo* studies also show that elevated plasma Hcy is a predictor of early mortality in older people[86]. *In vitro* research has demonstrated that exposure to Hcy significantly accelerates the rate of senescence in endothelial cells, perhaps by inducing chronic oxidative stress[87]. Hcy was observed to up-regulate expression of ICAM-1 and PAI-1, two cell-surface molecules that have been implicated in the pathogenesis of degenerative vascular disease[87-89]. Studies on mitogen-stimulated lymphocytes from older men showed a significant positive correlation between plasma Hcy concentration and MN measured using the CBMN assay[72], and a similar correlation was observed in cells from young men and women. These findings suggested that plasma Hcy above 7.5µmol/l, together with serum vitamin B12 concentration <300pmol/l, are associated with increased chromosome damage. Supplementation with an intake of folate and vitamin B12 above RDI reduced plasma Hcy and MNi in lymphocytes. The largest reduction in chromosome damage was observed at supplementation levels 3.5 times greater than the (then) RDI of 200µg/day, and mainly occurred in those individuals with above average levels of micronucleated cells prior to supplementation[72].

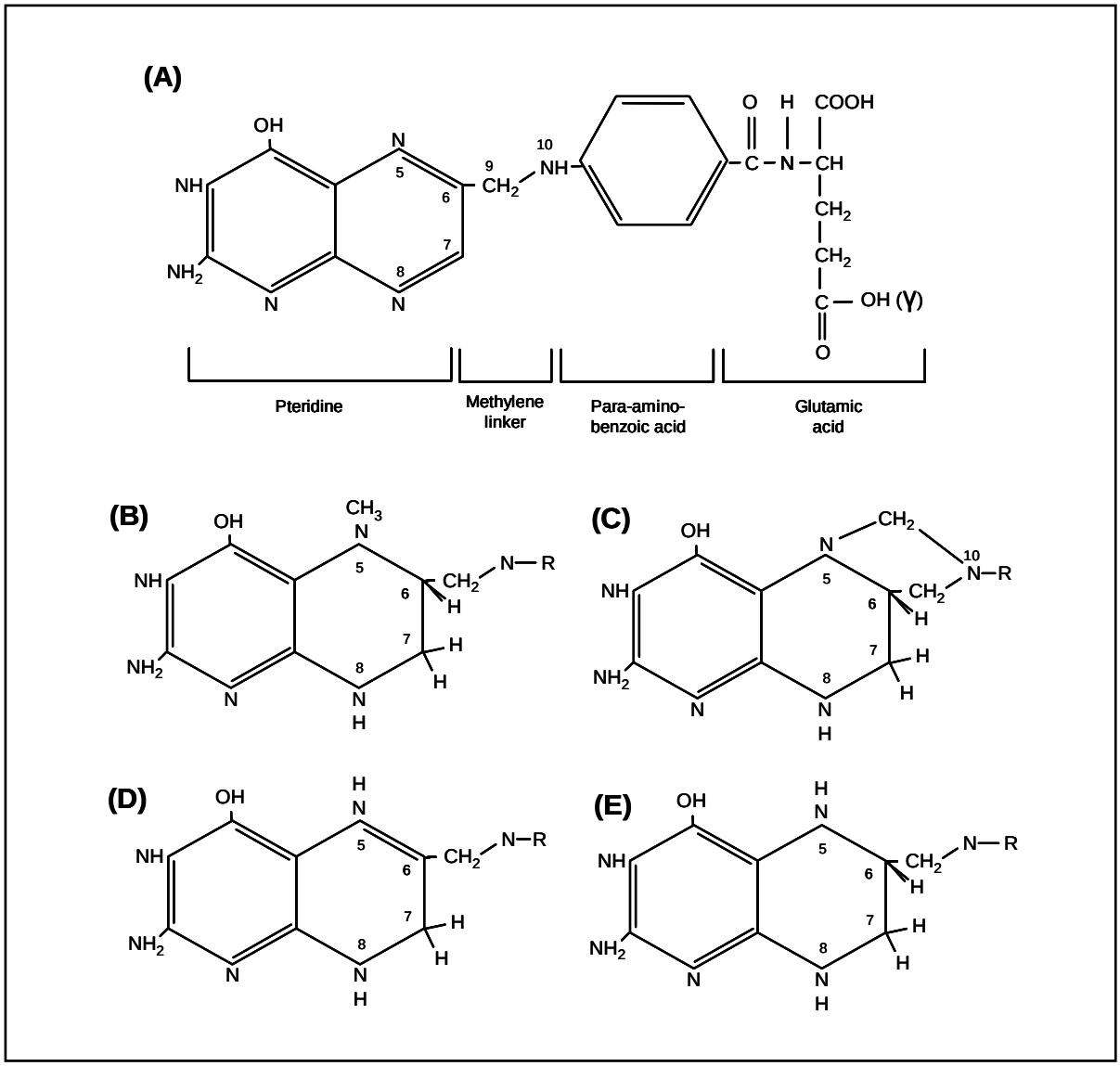

Figure 1.3 Chemical structure of folate

Folates are a family of compounds that have pteroylglutamate as a common structure (A). Additional glutamate residues are added via gamma peptide linkage at the γ-carboxyl group of the glutamic acid moiety[70]. Natural folate compounds exist in plasma and urine in a monoglutamate form, 5-methyltetrahydrofolate (5-MeTHF) (B), which can readily be transported across the cell membrane[71]. 5-MeTHF is then polyglutamated within the cell, where it enters the folate cycle. 5,10-methyltetrahydrofolate (5,10-MeTHF) (C) is the methyl donor responsible for methylation of dUMP to dTMP. Dihydrofolate (DHF) is formed when the pyrazine ring is partially reduced at carbons 7 & 8 (D), and tetrahydrofolate (THF) is formed when the pyrazine ring is fully reduced at positions 5, 6, 7 and 8 (E). Both DHF and THF play integral roles in the folate cycle, with THF being the active carrier of one carbon units within the cell[71].

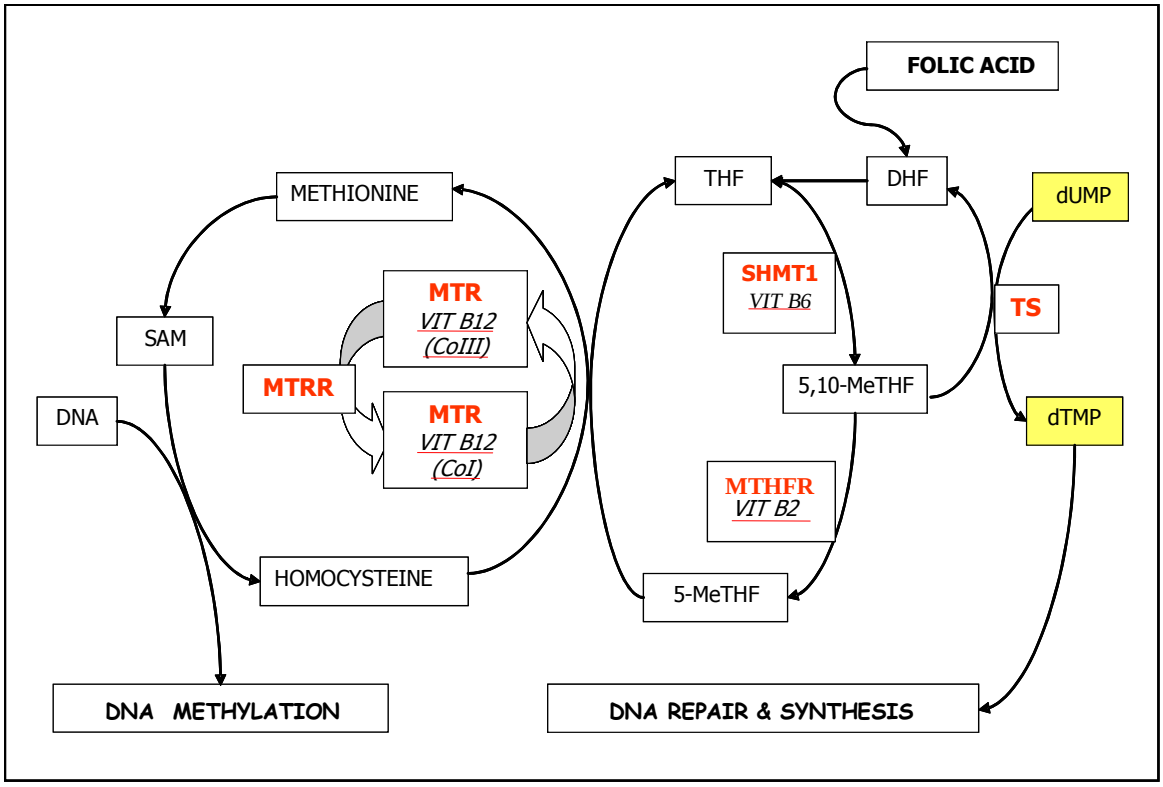

Figure 1.4 Folate pathway and genome maintenance

A simplified scheme of one carbon metabolism showing the effects of key enzymes (red text) and their respective cofactors (underlined) on DNA methylation, synthesis and repair. (B2, vitamin B2; B6, vitamin B6; B12, vitamin B12; DHF, Dihydrofolate; THF, Tetrahydrofolate; MTHFR, Methylenetetrahydro-folate reductase; MTR, Methionine Synthase; SAM, S-Adenosylmethionine; SHMT, serine hydroxymethyltransferase; dUMP, deoxyuridine monophosphate; dTMP, deoxy-thymidine monophosphate. (Adapted from Wang & Fenech, 2003[54]).

1.2.5 Genetic polymorphisms in the folate cycle

The ability of cells to uptake and utilise folate is dependent on the activity of enzymes in the folate/methionine cycle (Figure 1.4)[90]. Some examples include folate hydrolase, folate polyglutamate synthase, glutamyl hydrolase, proton-coupled folate transporter and reduced folate carrier[90]. Two key enzymes in the folate pathway that can affect Hcy concentrations in cells are methylene tetrahydrofolate reductase (MTHFR) and methionine synthase (MTR)[90,91]. Common polymorphisms in the genes encoding these enzymes (*MTHFR C677T, MTHFR A11298G, MTR A2756G*) have been shown to affect their activity and alter plasma Hcy concentration when folate is limiting. In addition, evidence has accumulated that genotypes encoding variations of these polymorphisms are associated with different rates of chromosomal instability, and that methylation status of DNA may be affected by particular polymorphisms[90].

Methylene tetrahydrofolate reductase (MTHFR) controls the bioavailability of folate for synthesis of dTTP, as well as for maintenance methylation of CpG[37,91]. The T allele of the *C677T* polymorphism, when homozygous, reduces activity of MTHFR by >50% and is associated with reduced risk for a variety of cancers. However, it is also associated with increased risk for cervical cancer, Down syndrome and neural tube defects[37,91]. Enzymic activity of MTHFR can be affected by feedback inhibition by SAM, or by a low concentration of its cofactor flavin adenine dinucleotide[37]. Homozygosity for the T allele (TT) impacts directly on the primary outcomes of the folate pathway, *ie.* formation of dTTP and DNA methylation. Reduction in MTHFR activity increases the concentration of 5,10-MeTHF and decreases the concentration of 5-MeTHF (Figure 1.3B). The latter should, theoretically, serve to decrease chromosome breaks induced by the action of glycosylase on uracil residues in DNA[74,92]. These observations indicate that in order to understand the effects of folate on the chromosome, it is important also to understand the impact of genotype.

1.2.6 Folate insufficiency and chromosome instability

Findings from a study in cultured human lymphocytes demonstrated that reduction of folate concentration (within the normal physiological range) from 120nmol/l to 12nmol/l resulted in chromosomal damage equivalent to that induced by acute exposure to 0.2Gray(Gy) of low linear-energy-transfer ionising radiation (*eg.* X-rays), a dose of radiation that is approximately ten times greater than the allowable annual exposure for radiation workers[35]. Low folate has also been associated with an increase in plasma Hcy levels and an increase in NPB in peripheral blood lymphocytes (PBL), the latter possibly arising from telomere end fusions[37,93]. Long term (9 day) cultures of primary human lymphocytes in 12, 24, 60 or 120nM FA verified that the concentration of FA correlated significantly and negatively with uracil in DNA and

with frequency of cells with MNi. These effects were reduced to a minimum at FA concentrations between 60 and 120nM[93], levels that are greater than the range of concentrations (10-30nM) observed in plasma in the normal population. It was also observed that the frequency of NPB and NBuds correlated significantly and negatively with FA dose, suggesting that chromosome rearrangement and gene amplification are also induced by folate deficiency[28].

Further *in vitro* studies using PBL from female volunteers have shown that low folate (12nM compared with 120nM) is also associated with significantly greater frequency of aneuploidy of chromosome 17 and 21, known risk factors for breast cancer and certain leukemias[94]. Folate status has also been shown to confer a protective effect with regard to DNA repair and stability following γ-irradiation[95]. WIL2-NS cells of lymphoblastoid origin were cultured in four different concentrations of FA for nine days, after which they were exposed to 1.5Gy of γ-irradiation. Frequency of radiation-induced micronucleated cells increased with decreasing FA concentration. Again, aneuploidy of chromosome 21 was found to increase with FA deficiency, but independently of ionising radiation. This study verified that folate status is an important modifying factor of cellular sensitivity to radiation-induced genome damage[95].

1.2.7 Folate insufficiency, uracil incorporation and telomeres

Folate is essential for transferring one carbon units in the *de novo* synthesis of nucleotides, specifically in the formation of dTTP from dUMP[74]. 5,10-MeTHF functions as a cofactor for the enzyme thymidylate synthase, which catalyses the conversion of dUMP to dTTP for incorporation of thymidine into DNA[74]. In the case of folate insufficiency, cytosolic concentrations of 5,10-MeTHF are reduced and this leads to an increase in the dUMP:dTTP ratio. DNA polymerase then incorporates uracil instead of thymidine into newly formed DNA strands, and during the repair of DNA[74]. Uracil glycosylase enzymes recognise and excise the aberrant base, generating a transient abasic site in one DNA strand[74]. Apurinic/apyrimidinic endonuclease (APE1) then acts on the abasic site, making a 5' nick in the backbone, prior to insertion of the correct base by DNA polymerase β, followed by ligation[96]. In situations where multiple uracil bases have been incorporated, the resulting single stranded nicks in the DNA may compromise the structural integrity of the telomere, and in turn, the chromosome. Uracil can also occur in DNA through the spontaneous deamination of cytosine residues and these, too, are removed through the BER process[97]. Dianov *et al* demonstrated in an *E. coli* model that the excision of two uracil bases, twelve bases apart on opposite DNA strands, had a ten-fold greater chance of inducing a double strand break, than the excision of a single uracil base[75]. This mechanism is thought to be responsible for the increase in chromosomal breakage

that has been observed under low folate conditions, and it can lead to chromosome instability and increased risk of diseases such as cancer. It is also likely to be the mechanism that is exploited in the use of methotrexate for treatment of tumours. This is based on the assumption that cancer cells have greater susceptibility to the effects of anti-folate agents than normal cells[74], thus suffering greater DNA damage and cell death than normal tissues of the body.

The inverse relationship between folate levels, incorporation of uracil and associated chromosomal damage was observed in human lymphocytes grown *ex vivo*[98]. After culture for ten days in medium containing low levels of FA (1ng/ml – 2µg/ml), the cells were treated with uracil glycosylase prior to harvest, and DNA damage analysed by the comet assay (a single cell gel electrophoresis method). It was found that DNA strand breakage and uracil incorporation increased with time and was greater at lower concentrations of FA[98]. A later study conducted by Mashiyama *et al* also used primary human lymphocytes and observed the effects of FA (0-3000nM FA) on uracil incorporation into DNA[99]. These researchers used an improved gas chromatography-mass spectrometry method to measure uracil and they found that the greatest amount of uracil incorporation into the DNA occurred in cells grown in the mid-range of FA concentrations. The lowest levels of uracil incorporation were observed at the highest concentration of FA (3000nM), although incorporation was also low in cells grown without FA). The authors showed that the low incorporation of uracil in cells grown without added FA was probably due to the low rate of cell division and DNA synthesis under these conditions[99]. Interestingly, these researchers also found a considerable spread in uracil incorporation in response to folate deficiency in cells from different donors, indicating that genetic background may play a critical role in the susceptibility of individuals to DNA damage and cancer risk[99].

As described above, results from *in vitro* studies on human cells show that there is an inverse dose-dependent correlation between concentrations of folate in the physiological range and frequencies of biomarkers of DNA damage, such as MNi (biomarker of double strand breaks) and NPBs (biomarker of chromosome fusions and/or breakage-fusion-bridge cycles)[93,95]. NPBs are expected to originate from dicentric chromosomes that arise from telomere end fusions and/or misrepair of DNA strand breaks. The findings highlight the possibility that folate deficiency, via uracil incorporation, may cause instability at the telomeric ends of chromosomes. Supporting this hypothesis, recent studies in yeast suggest that insufficient synthesis of dTTP from dUMP can result in shortened telomere length. This raises the possibility that excessive incorporation of uracil might cause breaks within the telomere sequence, as it can in other regions of the chromosome[100]. Similarly, oxidative stress in

mammalian and human cells is also associated with telomere shortening, possibly due to glycosylase activity leading to an accumulation of abasic sites and single strand breaks[101,102]. Consequently, the thymidine-rich nature of the telomere repeat sequence, low folate conditions may make the structural integrity of the telomere vulnerable, both *in vitro* and *in vivo*.

1.3 TELOMERES

Telomeres are nucleoprotein structures that cap the ends of chromosomes. The structural integrity of the telomere, and its characteristic hexamer repeat sequence ($TTAGGG_n$), is critical for protecting the ends of chromosomes from degradation and in maintaining overall genomic stability[103,104]. In differentiated cells, the number of DNA hexamer repeats is reduced during each cell division[105] due to the end-replication problem (see below). As a consequence, telomere length (TL) decreases in most differentiated cells throughout the lifespan of the organism[104]. Shortening of telomeres can result in chromosomal end fusions and an increased level of chromosomal instability (CIN), and this appears to be a key initiating event in cancers such as those of the lung, breast, colon and prostate, as well as in certain leukemias[6,106-110]. Telomere shortening has also been proposed to be one of the fundamental mechanisms that determine the rate of ageing in cells and whole organisms[111-113]. As discussed earlier, there is extensive evidence supporting an impact of dietary and environmental factors on chromosome stability[1,35,36,114-118]. However, there is limited knowledge of the impact of dietary factors on telomere length and structural integrity specifically. Given the pivotal role of telomeres in maintaining genome stability, it is important to assess the impact nutrients may have on telomere length and function. This knowledge would be relevant for developing strategies for use *in vivo* to prevent degenerative diseases of ageing, immune dysfunctions and cancer.

1.3.1 Telomere attrition

The work of Hayflick and Moorhead reported in 1961 challenged the previously held view that mammalian cells were immortal. These workers demonstrated that after 50-70 divisions in culture, differentiated cells suffer an irreversible loss of replicative capacity and appear to enter a state of senescence[119]. Despite being unresponsive to mitogenic stimuli, these cells remain viable for long periods of time[120]. In 1971 Olovnikov proposed that telomere shortening may be the mechanism responsible for the findings of Hayflick & Moorhead[121]. It was not until twenty years later that Harley *et al* published experimental evidence showing that the length of telomeres and the amount of telomeric DNA in human fibroblasts decreased progressively with serial passage *in vitro*, and possibly during ageing *in vivo*[122]. The 'end replication problem'

that is responsible for the senescence observed in dividing somatic cells is the result of approximately 50-200bp of telomeric DNA being lost at each cell division. This loss appears to be due to the inability of DNA polymerases to copy the final linear stretch of the lagging strand during DNA replication in S phase of the cell cycle[122-124].

Genome replication is effected by DNA polymerases, which lay down new DNA in a 5' to 3' direction. Replication of the lagging strand, which runs 3' to 5', requires small 'Okazaki' fragments of new DNA be formed by the 5' to 3' action of the polymerase. These are then joined by the enzyme ligase, to form a continuous strand. The leading strand, and every Okazaki fragment, must be initiated by an RNA primer, which is laid down by a primase enzyme. The primer facilitates binding of DNA polymerase, allowing extension of the new daughter strand. The RNA primer molecule is eventually degraded, and where this occurs within the chromosome the correct nucleotides are added to create a continuous daughter strand. At the end of a linear chromosome, however, DNA polymerase is unable to attach and fill in the missing bases following degradation of the RNA primer. Thus, the last few nucleotides at the 3' end of both the leading and lagging strands are lost with each round of cell division[104].

It is believed that when the shortest telomere in the cell reaches ~4kb in length a signal is activated for the cell to senesce or undergo apoptosis[124,125]. This replicative "clock" has been referred to as the Hayflick limit. It is thought to constitute an effective means by which cells that may have accumulated chromosomal aberrations during serial DNA replication no longer divide[126]. A study by Iwama *et al* in 1998 used Southern blot analysis to measure the size of telomere restriction fragments (TRF) in peripheral blood mononuclear cells from 80 individuals aged 4-95 years. It was found that up to 39 years of age, TRF decreased by approximately 84bp per year, while in individuals aged 40 and over the rate of TRF decrease had reduced to 41bp per year[127]. Rufer *et al* measured telomere length (TL) in 508 healthy donors aged 0 to 96 years, using the flow cytometric adaptation of FISH (flow-FISH method)[128]. Their results showed a significant decline in TL in PBL and granulocytes with age[128]. During the first year of life, telomere attrition occurred at a rate 30-fold higher than over the remainder of the lifespan[128].

The rate of telomere attrition has been shown to vary not only between age groups[127,129] but also between sexes[129,130]. Furthermore, it varies between chromosomes within a cell[129]. Individual chromosome arms have been found to have their own age-specific TL and erosion pattern, resulting in a high level of heterogeneity in TL[129,131]. On average, males have shorter

telomeres than females, and a faster rate of telomere attrition in all age categories [129,130,145]. It has been proposed that this is a factor that could contribute to the differences in life expectancy between the sexes[129,132]. The mechanism responsible for this effect of gender is not known, but there is some evidence that oestrogen may up-regulate telomerase[129,132,133]. The effect may disappear or be attenuated in post-menopausal women, but it is proposed that the lower attrition rate during the pre-menopausal years may be sufficient to ensure that telomeres remain longer throughout the life span in females[132].

Recently, evidence that environmental factors, such as psychological and physiological stress[102,134], cigarette smoking[135-137], obesity[137,138] and unhealthy lifestyles (low intake of fruit and vegetables, lack of exercise, high alcohol consumption)[130] contribute significantly to accelerated attrition of telomeric repeats. Exposure to reactive oxygen species (ROS) have been shown to result in shorter telomeres in fibroblasts *in vitro*[102], possibly due to strand breaks in the telomere sequence and/or disruption to telomere capping proteins[102,139]. An association has been made between telomere shortening and certain lifestyle factors that are known to either increase the level of ROS, and/or reduce the capacity of cells to manage ROS. For example chronic psychological stress has been shown to be significantly associated with higher cellular oxidative stress, lower telomerase activity, and shorter telomere length[134,140]. In a study conducted by Epel *et al*, it was found that PBL from healthy pre-menopausal women with the highest levels of perceived stress had, on average, shorter telomeres compared to those from low stress women[134]. Smoking has also been identified as an important risk factor for age-related disease associated with heightened oxidative stress[135-137]. In young men, a negative relationship has been observed between TL and smoking, and also with other markers of unhealthy lifestyle (high alcohol consumption, large waist circumference, low physical activity and low fruit and vegetable intake)[130].

While the work discussed above regarding lifestyle factors is compelling it is, nevertheless, circumstantial and others argue that TL, and the rate of TL attrition in individuals, is largely heritable[141]. Twin studies have shown that mean TLs are similar in monozygotic twins but differ significantly in dizygotic twins[142]. The TL in dizygotic twins were found to be highly conserved and stable throughout life, leading the authors to conclude that environmental contributions are not important with respect to TL and longevity[141]. There is also evidence that the paternal influence on TL of the offspring is significant[143-145]. TL in sperm is known to increase as the male ages, and a positive correlation has been shown between the paternal age and the TL in their children. This suggests that vertical transmission of TL may contribute significantly to TL variations in the population[145]. Graakjaer *et al* (2004) also showed that

chromosome arms of identical genetic origin have similar relative TL in both parents and offspring[146]. Taken together, these findings suggest that chromosomal TL of the parents has overarching importance among the factors that contribute to TL variation in the population[146].

1.3.2 Telomere structure and capping proteins

The ends of eukaryote chromosomes are comprised of the telomeric 'cap' and a sub-telomeric region that provides a buffer between the telomere and the gene-rich coding region of the chromosome[147]. While detail regarding the composition of the sub-telomere is yet to be fully elucidated, it is defined as a region approximately 500kb in length that is known to consist of telomeric $(TTAGGG)_n$-like repeats, sub-telomeric repeating sequences, segmental duplications, and satellite sequences[147]. In contrast to the telomere, the sub-telomere also contains a low density of genes[148].

The telomere in human lymphocytes, on the other hand, comprises approximately 8-15kb of a repeating hexamer sequence $(5'\text{-}TTAGGG\text{-}3')_n$[104]. A series of protein complexes bind to this region of repeats in a process referred to as 'capping', thus forming a higher order structure that 'caps' the telomere (Figure 1.5)[103]. Chromosome capping provides structural integrity and protection to the telomere and involves multiple interactions between different molecular components[149]. A significant component of functional capping is the shelterin (also known as telosome) complex[103]. This complex is comprised of six proteins, three of which bind directly to DNA, namely telomere repeat binding factors-1 and -2 (TRF1 and TRF2), and 'protection of telomeres-1' (POT1)[103,149,150]. TRF1-interacting nuclear factor-2 (TIN2), Repressor/activator Protein (RAP1), and TPP1 (previously TINT1, PTOP or PIP1) are the three additional proteins that make up the telosome, however, the latter do not interact directly with telomeric DNA (Figure 1.5)[103,150].

TIN2 and TPP1 are critical for the assembly of a functional telosome, while RAP1 forms part of a complex with TRF2. TIN2 is the linchpin of the shelterin complex, providing a link that associates TPP1/POT1 with TRF1 and TRF2. TIN2 also links TRF1 and TRF2, thus contributing to the stability of TRF2 binding to telomeric DNA[103]. The TIN2/TPP1 complex has also been shown to provide a molecular mechanism by which TRF2 alone can maintain telomere length homeostasis, in the absence of TRF1[151]. As telomeres shorten with each cell division, the capping structure is also reduced in size. It is believed that either senescence or apoptosis is triggered when the capping structure is reduced to a critical level[103]. Recent *in vitro* work in mitogen-activated normal T lymphocytes showed a transitory increase in telomerase activity, in association with a decrease in expression of shelterin genes, following

each round of stimulation[152]. Reduced capping was also associated with an increase in the early markers of a DNA damage response; γH2AX and 53BP1, and an increase in the percentage of cells with damage foci in telomeric DNA[152,153].

At the 3' end of each telomere is a G-rich tail. This single stranded DNA consists predominantly of guanine residues and is approximately 100-300bp in length[154]. This tail intercalates into the duplex region at the end of the telomere, forming a closed T-loop, and a smaller D-loop structure (Figure 1.6)[154-157]. The T-loop protects the telomere from degradation by nucleases and minimises the possibility that it will be mistaken for a double-strand break requiring repair[158], while the D-loop appears to consist of the displaced strand from the dsDNA[156]. POT1 binds directly to the ssDNA of the overhang, and is suggested to be involved in the regulation of G-tail length. This suggestion is based on evidence that there is shortening of the overhang when expression of POT1 is reduced[159]. POT1 also associates with TPP1 to form a heterodimer that has enhanced affinity for telomeric ssDNA, compared with POT1 alone[157]. TPP1 provides a physical link between telomerase and the telosome complex, thus regulating the process of telomere lengthening[157]. Early work by Wellinger and co-workers in yeast showed the G-tail to be regulated during the cell cycle, with lengthening during S phase[160-162]. More recently, Lee *et al* (2008) have shown that the length of the G-tail is highly heterogeneous[154]. This group measured the G-rich 3' overhang in 56 human cancer cell lines and found a 23-308% variation relative to the length in HeLa cells, whereas the range was 92-202% in five non-neoplastic cell lines[154]. G-tail length correlated positively with the length of telomeres in these cells, but there was no correlation between G-tail length and levels of mRNA encoding hTERT, the catalytic subunit of telomerase[154].

Both TRF1 and TRF2 form homo-dimers via the TRF-homology domain[163-165], and they bind directly to telomeric dsDNA via a myb domain[166]. TRF1 is a multi-protein complex that incorporates Tankyrase 1 and other poly(ADP-ribose) polymerase (PARP) molecules that play a role in negatively regulating the maintenance of telomere length[167]. Over-expression of dominant-negative TRF1 molecules results in telomere elongation[168]. Given that there was no measurable change in telomerase expression, these researchers concluded that TRF1 controls telomere elongation by mechanically blocking access to telomerase[168]. Work recently published using a transgenic TRF1 mouse model supports the earlier findings that TRF1 acts as a negative regulator of TL, because over-expression results in telomere shortening *in vivo*[169].

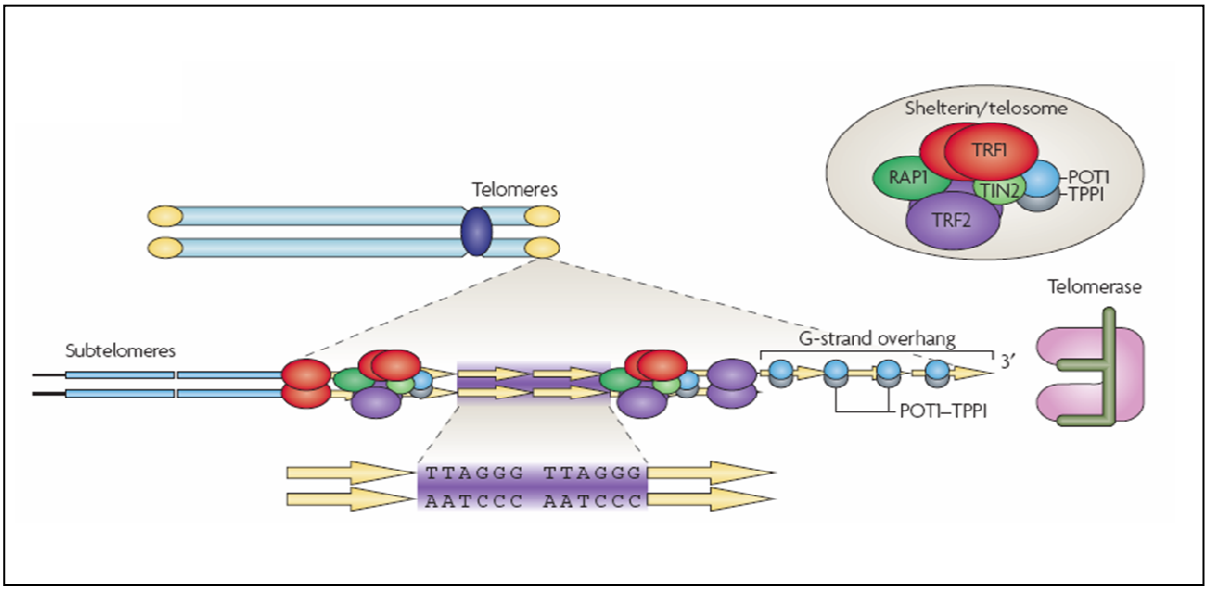

Figure 1.5 Structure of telomeres and subtelomeres in mammals

Double stranded telomeric repeats are bound by a multiprotein complex known as 'shelterin' or the 'telosome', which comprises the telomere binding factors TRF1 and TRF2, TIN2, RAP1, POT1 and TPP1. The G-strand overhang is also bound by the POT1-TPP1 heterodimer. Telomerase is able to recognise the 3' end of the G-strand overhang to elongate telomeres. (TRF, telomere repeat binding factor; TIN2, TRF1-interacting nuclear factor 2; RAP1, repressor-activator protein 1; POT1, protection of telomeres 1; TPP1, previously TINT1, PTOP or PIP1). (Adapted from Blasco, Nature Reviews Genetics, 2007[148])

This latter study also showed that TRF1 over-expression leads to increased chromosomal end fusions and telomere recombination, suggesting a possible role of TRF1 in the mitotic spindle checkpoint[169]. Inactivation of TRF1 has been shown to disrupt localisation of other telosome components to the telomeres, resulting in overall chromosomal instability[170]. TRF2 is critical for telomeric integrity, with more than 100 copies coating the full length of human telomeres at all stages during the cell cycle[166,171]. This protein is primarily responsible for protecting the chromosome ends from being recognised as double strand breaks by the DNA repair machinery, thus preventing end-to-end chromosome fusions[172,173]. It is likely that this protection is achieved through interactions of TRF2 with DNA-damage signaling and repair factors[174,175]. Studies have been performed using a dominant negative TRF2 molecule, which dimerises with endogenous TRF2 and disabling not only its own capacity to bind dsDNA, but also the binding of other factors which interact indirectly via TRF2[172]. TRF2-depleted telomeres led to the activation of the ATM/p53 response pathway, suggesting that uncapped telomeres are misinterpreted as sites of DNA damage[172,176]. It was also found that inhibition of TRF2 resulted in fusions between a substantial fraction (~15%) of telomeres[172]. This appeared to arise from loss of the 3' G-strand overhang, which shortened progressively after loss of bound TRF2, the process requiring several cell divisions to reach a 50% reduction in length of the overhang[172]. More recent studies have shown that single strand break repair mechanisms are impaired by TRF2, suggesting that the role of bound TRF2 is to sterically hinder access by both DNA repair machinery and telomerase[177].

1.3.3 Maintenance of telomere length; telomerase and the ALT mechanism

The shortening of telomeres within actively dividing somatic cells is due to degradation of RNA primers at the 3' ends of chromosomes[104]. It is essential, however, that the maximum telomere complement is maintained in stem cells and germ cells, where chromosome integrity is paramount. The mechanism responsible for counteracting telomere attrition involves the enzyme telomerase, which extends telomeres by adding hexamer $(TTAGGG)_n$ repeats to the 3' end of chromosomes and thus maintains telomere length at ~15kb in these cells[178,179]. The level of expression of telomerase, and activity of the enzyme, varies between different cell types, and at different points in the cell cycle[180]. While substantial levels of hTERT are expressed in stem and germ cells, only very low levels are detectable in somatic cells[181].

The active telomerase complex in humans comprises a dimer, each component consisting of three subunits; a reverse transcriptase catalytic subunit (hTERT), a 451nt RNA molecule (hTR, aka TERC) containing the template for telomere repeat addition, and the protein dyskerin[182]. The telomerase dimer binds directly to ssDNA at the 3' end of the chromosome, and this is

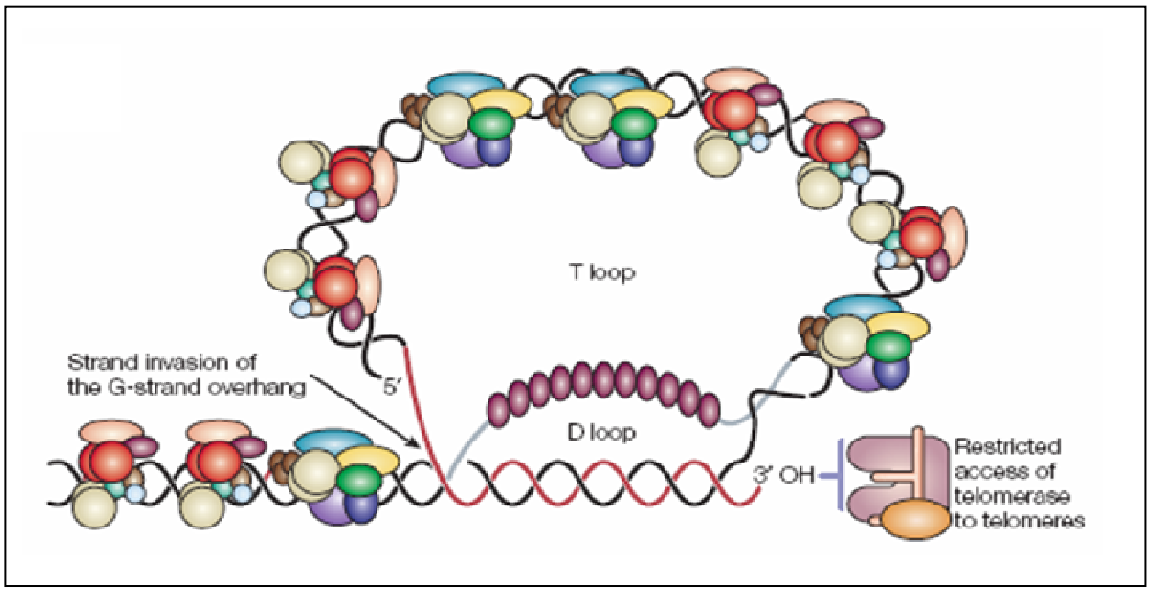

Figure 1.6 Telomere T-loop conformation

At the 3' end of each telomere is a G-rich tail, approximately 100-300bp in length[154]. This tail intercalates into the duplex region at the end of the telomere (highlighted in red), forming a closed T-loop, and a smaller D-loop structure[154-157]. The T-loop protects the telomere from degradation by nucleases and minimises the possibility that it will be mistaken for a double-strand break requiring repair[158], while the D-loop appears to consist of the displaced strand from the dsDNA[156]. (Adapted from Blasco, Nature Reviews Genetics, 2005[167])

where addition of telomere repeats occurs[182,183]. While the detail surrounding recruitment of the telomerase complex to the telomere is not fully elucidated, it has been shown that the complex exhibits a significant preference for shorter telomeres[183]. The amount of bound enzyme can be increased by inhibiting telomere binding proteins such as TRF1 and TRF2, or by generating increased cellular levels of telomerase[183]. Enzymic activity is regulated at numerous levels, including through the expression of the hTERT catalytic subunit. There is also recent evidence that TelRNA (telomeric RNA, also known as telomere repeat-containing RNA repeats (TERRA)) molecules may inhibit telomerase activity, possibly by blocking the RNA template[184]. Transcription of TelRNA is silenced in cells where telomerase has been reactivated, suggesting an inverse relationship between the levels of telomerase and TelRNA[184]. TelRNA molecules are heterogeneous in length and are transcribed from several sub-telomeric loci[185]. They appear to associate with telomeric heterochromatin[185], and are expressed at levels that are proportional to telomere length[186].

Telomerase dysfunction has been directly associated with numerous disease states. Both the TERT and hTR subunits have been implicated in adult-onset[187] and idiopathic pulmonary fibrosis[188], aplastic anemia[189-192] and autosomal dominant dyskeratosis congenita. In the case of the latter, the primary causative factor is frequently a dysfunctional form of TERT[188-190]. Defective hTR is one mechanism thought to underlie myelodysplastic syndrome[193-195], while TERT has been implicated in coronary artery disease[196].

Late stage cancer cells often have very short telomeres, indicative of their long proliferative history[104]. Nevertheless, 80-90% of these cells have been shown to have active telomerase, which is thought to facilitate their immortality[167,197]. As a result, strategies to block the production or activity of telomerase are of great interest in experimental cancer therapy. These strategies have the advantage that they could target cancer cells, without affecting healthy somatic cells[198]. However, the effect of blocking telomere maintenance in healthy stem cells must also be evaluated.

An alternative mechanism for maintenance of telomeres, known as ALT, also exists whereby DNA from one telomere anneals with the complementary strand of another, acting as a primer for synthesis of new telomere repeat sequences[197]. This homologous recombination (HR)-based mechanism has been shown to be active in only a small fraction (~5%) of telomerase-negative cancer cells, and in some circumstances may also be present in parallel with active telomerase[197]. The mechanisms underlying the ALT+ phenotype are not well understood, but features include increased levels of sister chromatid exchange involving telomeric sequences

(T-SCE), highly heterogeneous telomere length, and the presence of ALT-associated promyelocytic leukemia bodies (APBs) where telomeres have been shown to co-localise with recombination-associated proteins[199].

1.3.4 Telomere length regulation and disease

Telomere shortening due to normal cellular ageing is well documented in blood cells and cells in many tissues[7,128]. However, accelerated change in TL (predominantly shortening) relative to rates of shortening during normal ageing has been observed in numerous cancers and other disease states[2,7,200]. Aberrant shortening, or compromise, of telomeres has been shown to result in chromosome instability (CIN), as evidenced by increases in end-to-end fusions, BFB cycles, aneusomy and chromosomal aberrations[201]. Telomere-associated CIN has been shown to lead to loss of cell viability *in vitro*, while *in vivo* it has been associated with ageing-related pathologies such as heart failure, immuno-senescence (infections), digestive tract atrophies, infertility, reduced viability of stem cells, reduced wound-healing and loss of body mass[167,202]. Significantly shortened telomeres have been reported in a diverse range of conditions, including depression[203], cognitive decline/dementia[204], Alzheimer's Disease[205], atherosclerosis[206] and cardiovascular disease (CVD)[207], Types 1 and 2 diabetes[208,209], rheumatoid arthritis[210] and chirrhosis of the liver[211]. Several genetic disorders associated with telomere maintenance all show telomere shortening to be associated with accelerated degeneration and ageing and the development of disease, including cancers (see Chapter 1.3.4.3 below)[6,7]. Extensive evidence supports the notion that loss of TL regulation, predominantly telomere shortening, may be a key initiating factor in genomic instability, which triggers detrimental changes to the integrity of the chromosomes and thence disease[7,212,213].

Meeker *et al* explored TL abnormalities in intraepithelial neoplasia lesions and confirmed that 95% of the 196 lesions analysed showed TL alterations: 92% had shortened TL, 7% showed TL elongation, and 5% displayed both shorter and longer telomeres[212]. A recent review by Svenson *et al* also found a high level of heterogeneity in TL in malignant tissues[2]. Studies in yeast have suggested that up to 150 genes may be involved in control of TL, directly or indirectly[214,215], providing a possible explanation for the heterogeneity of TL that has been observed in different tissues, blood cells and tumour types[2]. These studies provide important evidence that telomeres are dynamic structures, controlled by multiple factors which are yet to be fully determined.

1.3.4.1 Telomere length in malignancies

Investigations into TL in haematological malignancies (myelodysplasia, acute myeloid leukemia (AML), chronic myeloid leukemia (CML), chronic lymphocytic leukemia (CLL) and myeloma) have consistently found shorter telomeres to be positively associated with disease evolution and with poor prognosis[2,216-219]. TL in solid tumours, on the other hand, is highly heterogeneous, with prognostic significance of shortened or elongated telomeres varying between different tumour types[2,213]. A unifying factor for all data on solid tumours is that the larger the variation of mean tumour cell TL from the TL in benign tissues, the stronger the correlation with poor disease outcome[2].

Only a small percentage of studies have shown telomere elongation in tumour, relative to non-tumour, tissue[2,220-222]. Longer TL tends to be observed in more advanced stages of disease and has been positively correlated with poor prognosis in hepatocellular[220], colorectal[223,224], Barrett (esophageal)[225] and head and neck tumours[2,221]. It is speculated that the increase in TL may be due to increased telomerase activity in late stages of disease, as was demonstrated by Oh *et al* in hepatocellular carcinoma[220]. This is also consistent with previous reports that CIN in pre-neoplastic cells with short telomeres is stabilised by the activation of telomerase[226].

The significant proportion of reports on TL and malignancies, however, show TL shortening to be positively associated with poor prognosis[2]. In just one example tissues from 49 invasive human breast tumours were divided into three groups based on telomere content relative to a standard placental tissue[107]. Tumours with the least amount of telomeric DNA had the highest levels of aneuploidy and metastasis, both of which are features associated with poor outcomes[107]. Similar reports, whereby short telomeres in tumour tissues have been associated with poor outcomes (including tumour recurrence, metastases and death), have been shown in breast[107,227-229], prostate[230,231], colorectal[223,224], lung[232-234], oesophageal[225], and renal cancers[2,235]. Interestingly, poor lung cancer[233,234] and neuroblastoma prognoses[222,236] have also been associated in separate studies, both with short and long TL in tumour tissues. These findings further highlight the significant degree of heterogeneity in TL, even within the same cancer type.

1.3.4.2 Telomere length as a prognostic marker for malignancies

At this stage it is unclear whether TL measurements in PBL have value clinically as predictors of cancer outcomes. One study has reported an association between short mean TL in PBL with an increased risk of cancers of the bladder, head and neck, lung and renal cells[237]. Whereas a large longitudinal study carried out in 959 individuals over 10 years showed no

differences between TL in PBL from 343 individuals who developed cancer from those that were clinically normal[238]. It is unclear whether TL dynamics of blood cells are secondary, in response to the cancer, or whether changing TL is a reflection of a more general dysfunction of telomere regulation that may predispose an individual to cancer[2]. TL in blood cells may be determined by the proliferative vigor of the patient's T cells when exposed to cognate antigen, or the rate of turnover of immune cells may be increased in the presence of a cancer, potentially impacting on TL attrition and presenting as accelerated telomere shortening[2].

The issue is further complicated by the differing relationships observed between TL of blood cells from patients with solid tumours, and the tumour tissue itself [2]. TL in PBL from 265 newly diagnosed breast cancer patients (pre-treatment, post surgical removal of tumours) was found to be significantly longer than TL of PBL from 446 control patients[239]. Furthermore, findings from this study showed that long telomeres in PBL of this cohort was predictive of poor outcome, as those patients with shorter telomeres in PBL showed increased survival rates[239]. Similar observations were reported for patients diagnosed with clear cell renal carcinoma, where the prognosis was significantly poorer for patients whose PBL had the longest TL, compared with those with shorter PBL TL[235].

1.3.4.3 Telomere-associated genetic disorders

Defects in human genes associated with telomere biology have been shown to cause genome instability syndromes, hallmarks of which include accelerated telomere shortening, increased predisposition to cancer and premature ageing[6,7]. Some examples of these include Werner and Bloom syndromes, aplastic anaemia, Ataxia telangiectasia, Nijmegen breakage syndrome, Fanconi Anemia and dyskeratosis congenita[6,167,240].

Sufferers of Werner syndrome display premature ageing and increased incidence of cancers. Predisposition to these cancers arises from a mutation in the gene encoding the RecQ helicase, WRN, which has multiple roles in DNA replication, repair and recombination[240,241]. WRN helicase is required for replication of the G rich telomere region, and as a result, WS cells exhibit dramatic loss of telomeric repeats, increased chromosomal instability, activation of the DNA damage response and end fusions of chromosomes[240]. In culture, primary fibroblasts from Werner syndrome patients display a shorter lifespan relative to cells from healthy donors and this phenotype can be rescued by transfection of a construct encoding telomerase[240].

Bloom syndrome is a rare recessive disorder that is associated with growth retardation, immunodeficiency and increased risk of malignancy. The pathology arises from a defect in the

BLM protein, which has sequence similarities with the RecQ subfamily of helicases[6]. Bloom syndrome cells show marked genomic instability, including hyper-recombination between sister chromatids, and telomere fusions[6].

Ataxia telangiectasia (AT) is another rare autosomal recessive disease. The features of AT are due to a mutation in a tumour suppressor gene that produces in these individuals a functionally defective polypeptide known as the ataxia-telangiectasia mutated (ATM) protein (see 1.4.1 below). The clinical phenotype is complex and it is associated with shortened telomeres and genomic instability[6]. The functionally normal homologue of the ATM protein is a key component of the early response to DNA damage and it is important for repair of DSBs, thus reducing the risk of genome instability and cancers[242]. Due to mutations in this gene, AT patients are hypersensitive to X-rays and γ-rays because of their inability to detect and facilitate DSB repair[242]. The predominant clinical features of the disease include neuronal degeneration, immunodeficiency, premature ageing, and cancer predisposition (particularly lymphomas and leukaemia)[6]. At the cellular level, AT fibroblasts undergo premature senescence *in vitro* and display high levels of chromosomal end fusions as a result of accelerated telomere shortening[6].

Dyskeratosis congenita (DK) is a disorder characterised by unchecked telomere loss in haematopoietic stem cells, resulting in bone marrow failure[243]. It is a heterogeneous inherited condition associated with dysfunction of telomerase[243]. Fanconi anaemia is another rare autosomal recessive genetic disorder in which progressive bone marrow failure is a feature. The disease is characterised by developmental defects, progressive bone-marrow failure and a high risk of both acute myeloid leukemia and solid tumors[6]. At least twelve genes have been implicated in the aetiology of Fanconi anaemia[6]. Telomere shortening has been observed in peripheral blood samples from these patients, together with a high proportion of extra-chromosomal TTAGGG sequences and a significant increase in telomeric fusions compared with healthy individuals[6,244]. This latter feature resembles the genetic damage observed in AT. Excessive telomere breakage has been linked to defects in oxygen metabolism, with oxidative damage causing excessive formation of 8-oxodG, which is known to accelerate telomere shortening[6].

1.4 TELOMERES AND THE DNA DAMAGE RESPONSE (DDR)

Different types of insults result in different forms of damage to the DNA structure[245]. Intrinsic damage, such as spontaneous base modification or replication errors, may occur and lead to base-pair mismatch, insertions or deletions of bases, or single strand breakage. Endogenous oxygen radicals or exogenous chemical agents can cause base modification, abasic sites, DNA adducts, cross-linking or strand breakage. UV or ionising radiation, on the other hand, may lead to formation of pyrimidine dimers, base modifications, abasic sites and strand breaks[245]. The coordinated cellular response must be appropriate to the specific form of damage. The DNA damage response (DDR) involves two key processes; the damage checkpoint response (which facilitates a pause in the cell cycle until damage has been resolved) and DNA repair pathways[246]. Where damage is excessive or irreparable, the apoptotic pathway may be activated, or the cell may enter a senescent state[245]. If repair processes are defective, however, resulting mutations and chromosome aberrations may lead to malignant transformation of the damaged cells[245].

Many components of DDR pathways interact either with components of the shelterin complex, or directly with telomeric DNA and they have been implicated in telomere homeostasis in both yeast and mammalian models[246,247]. Some examples of components that have been studied in humans include ataxia-telangiectasia mutated (ATM), the MRN complex (MRE11/Rad50/Nbs1), WRN, PARP-1/2, RAD51D, BRCA1, ERCC1/XPF, the Ku complex and DNA-PKcs[246-248]. Deletion and mutation studies have shown that all of these factors impact on telomere length or integrity. However, details of the mechanisms involved have not been fully determined[246,247].

1.4.1 DNA damage checkpoint response

Studies conducted by d'Adda di Fagagna *et al* have demonstrated that critically short telomeres activate 'telomere-initiated senescence'; a permanent cell-cycle arrest facilitated by proteins of the DNA damage checkpoint pathway[249,250]. The arrested state continues until the damage has been resolved and the cell is able to resume replication and mitosis. Where damage cannot be repaired, the cell either enters a state of replicative senescence, or undergoes apoptosis[249,250]. Telomere shortening and the associated reduction in capping, loss of the 3' G-tail, or telomere breakage can all result in the chromosome end being mis-identified as a DSB. The initial cellular response to a DSB is activation of a DNA damage checkpoint pathway and arrest of cell cycle progression while repair mechanisms are enlisted[249].

Checkpoint pathways involve a cascade of reactions, the primary effect of which is activation of effector proteins by phosphorylation and acetylation. Two factors which are pivotal to the initiation and regulation of a checkpoint response at G1/S, intra-S and at G2/M phases are the ATM and ataxia-telangiectasia related (ATR) kinases[242,246]. These proteins are both members of the phosphatidyl inositol-3 kinase family and appear to have distinct but overlapping functions[246]. ATM primarily responds to DSBs generated by agents such as ionising radiation, while ATR responds to a wider range of lesions, and appears to be of particular importance in response to damage during S phase[246]. The MRN complex acts as an initial sensor for DSB breaks, recruiting ATM to the site of damage. Recruitment is effected by the binding of ATM to the C-terminal domain of Nsb1 (part of the MRN complex). This leads to auto-phosphorylation of ATM, which is followed by dissociation of the inactive dimeric form to give rise to the active phosphorylated monomer[242]. Activated ATM in turn phosphorylates mediators that include BRCA1, MDC1 and 53BP1, which then activate the signal transducer kinases CHK1 and CHK2 and these target DNA repair or cell cycle control effector proteins such as p53[242,246]. One example of such a pathway is the arrest of cell cycle at G1/S by ATM-dependent phosphorylation of Chk2, which in its activated form is involved in stabilising p53. Stabilisation of p53 leads to transcriptional induction of p21, which associates with Cdk2-cyclin E kinase, inhibiting it and preventing cell progression into S-phase[242].

1.4.2 DNA damage repair

The four main DNA repair pathways in human cells are non-homologous end joining (NHEJ), homologous recombination (HR), nucleotide excision repair (NER) and base excision repair (BER). Different types of damage trigger the recruitment of the factors that are appropriate for the specific response required[247]. In addition to being critical for activating a checkpoint pathway, ATM and ATR play a central role in recruiting factors for DNA repair by mediating phosphorylation at serine 139 on histone 2A on either side of the site of DNA damage. This forms γ-H2AX, which is an early stage marker of a DSB[246]. γH2AX is believed to be important in facilitating the assembly of checkpoint and DNA repair factors at the damage site[246,249].

NHEJ and HR are the two principal pathways for repair of DSBs, and these are highly conserved throughout eukaryotes[246]. NHEJ is the primary pathway for DSB repair for breakage at telomeres in mammalian cells, while single-celled organisms such as yeast rely on HR[246]. The latter requires the presence of an undamaged homologous partner to allow strand exchange and extension and it is reliant on the MRN complex[245]. In contrast, the NHEJ mechanism facilitates the ligation of any two exposed double strand DNA molecules[246]. NHEJ

is a rapid "emergency" response and it is known to be error prone. Such errors lead to the formation of asymmetrical chromosome rearrangements, with frequent micro-deletions[245]. NHEJ is also an essential component of the V(D)J recombination process in developing T cells and B cells, where it is involved in the re-ligating of DNA during rearrangement of the genes encoding the T-cell receptor and immunoglobulin[245,251]. The key factor essential for NHEJ is the heterodimer Ku (Ku70 and Ku80), which detects the broken ends and recruits DNA-dependent protein kinase catalytic subunit (DNA-PKcs)[245,252,253]. The break is then joined by DNA ligase IV and X-ray cross-complementing-4 (XRCC4)[245,252,253]. It has been proposed that Ku acts as a factor to prevent uncontrolled access of telomerase to both internal DSBs and to telomeres[248]. As such, telomeres may be critical sites for damage surveillance, due to the importance of telomeres in preventing CIN. DSB repair proteins may balance repair activities and telomere maintenance and thus serve as key regulators of chromosomal integrity[248].

Nucleotide excision repair (NER) is a repair process responsible for resolving lesions that distort the helical structure of DNA[254]. UV light and polycyclic aromatic hydrocarbons are examples of insults that can result in bulky adducts (such as dimers) that require excision and repair of more than one nucleotide[255]. NER is divided into two sub-pathways: transcription coupled (TC-NER) and global genome (GG-NER). The primary difference between these pathways is the mechanism by which the lesion is initially recognised[254].

Base excision repair (BER), on the other hand, is responsible for recognising and repairing single nucleotide DNA lesions that could result in mutagenic or cytotoxic effects. Such lesions include abasic sites, DNA single-strand breaks, and modified bases such as those that occur when uracil is incorporated in place of thymine or when small adducts such as 8-OH-dG are formed due to oxidative stress[256]. Proteins of the BER act in a coordinated, cooperative manner to excise and replace the inappropriate base, clean up the terminal end(s) and seal the final nick[256]. Glycosylase enzymes (*eg.* uracil glycosylase) excise the inappropriate base by catalysing hydrolysis of the N-glycosidic bond, leaving an abasic site with the phosphodiester backbone intact[256]. Apurinic endonuclease 1 (APE1) mediates the process, in cooperation with DNA polymerase β, which replaces the excised nucleotide[256]. Sealing of the nick on either side of the new nucleotide is achieved by a complex of XRCC1 and DNA ligase 3α, or by DNA ligase 1[256].

1.4.3 Replicative senescence

When DNA damage is too widespread or too severe for successful repair, the cell may undergo apoptosis or enter a state of replicative senescence. While the precise conditions that dictate

the fate of the damaged cell are unclear, some evidence suggests that senescence is triggered by a protracted DDR[250]. Following successful repair of a DNA lesion, DDR foci are dissembled, primarily through chromatin remodelling and the dephosphorylation of γH2AX[250]. As such, promptly repaired lesions are expected to lead to transient and relatively small DDR foci, whereas more severe damage will stimulate more protracted DDR signalling and increased numbers of γH2AX foci. It is this large and prolonged damage signal that is believed to trigger the transition from a checkpoint pause in the cell cycle to an irreversible halt in replication[250]. Telomere shortening is a known trigger of senescence, and it is believed to be an inbuilt protection mechanism to ensure that uncontrolled proliferation of ageing and potentially aberrant cells does not occur. As telomeres shorten, the number of capping proteins (TRF1 and TRF2) at the ends of chromosomes is also reduced. As capping is known to inhibit the recruitment of DDR proteins, a reduction in TRF1 and TRF2 can lead to an increase in ATM/ATR binding at the telomere. Experimental evidence using chromatin immuno-precipitation (ChIP) assays supports this theory, whereby critically short telomeric DNA sequences are shown to be tightly associated with DDR factors[249,257]. It is believed that senescence is not reversible *in vitro*, either by altering the cellular environment, removing cell contact inhibition or by providing abundant nutrients[250].

1.4.4 Proteins of the DDR and telomere homeostasis

Experimental evidence in both yeast and mammalian models indicate that proteins involved in the DDR have significant roles in telomere homeostasis[246,247]. Inactivation of ATM in the disease AT, for example, results in defects in control of telomere length control and in extreme telomere shortening[258]. Other checkpoint PIKK (phosphatidylinositol-3 kinase-related kinases) proteins have also been shown to cause loss of control of telomere length and instability of telomeres in yeast models[259,260]. Inactivation of either component of the Ku heterodimer was found to lead to telomere shortening in both *S. cerevisiae* and *S. pombe*[261-263]. Interestingly, the shortened telomeres then stabilised at the new, shorter length with no further attrition[261]. Later studies demonstrated that Ku is physically associated with mammalian telomeres *in vivo*[264,265], and that human Ku interacts with both TRF1 and TRF2, suggesting that it has a role in TL regulation[266-268]. Both Ku and DNA-PKcs have been found to be essential for maintenance and integrity of telomere capping[269,270]. How these factors impact on telomeres is not fully known. It has been hypothesised that they may facilitate the phosphorylation of other factors required for telomere homeostasis, that they may act to alter the conformation of telomeric chromatin, or that they might influence access of telomerase and/or activity of the enzyme[246].

1.4.5 The impact of telomere position effect (TPE) on DNA repair

Studies in yeast have demonstrated that DSB repair is deficient in telomeric regions, possibly due to differences of (non-histone) chromatin structure in these regions[271]. Experimental introduction of DSBs by endonucleases at different sites in chromosomes demonstrated that DSBs near telomeres are not repaired efficiently by NHEJ, but instead result in complex chromosome rearrangements[271]. Results from a study in *S. cerevisiae* indicated that telomeric repeats confer an "anticheckpoint" effect[272]. It was found that an internal tract of telomeric repeats adjacent to DSBs inhibited DNA damage checkpoint signalling. A DSB at other sites led to cycle arrest lasting 8-12 hours, but a DSB adjacent to telomeric DNA lasted for only 1-2 hours[272]. This anti-checkpoint effect was observable on DSBs located up to 0.6kb from the telomeric DNA. The authors proposed that telomeres contain proteins that inhibit the initiation of checkpoint signalling by nearby DNA breaks[272]. It has also been shown that mammalian telomeres are deficient in repair of single-strand breaks and damage from UV light[273,274]. Together, these observations suggest that single or double strand breaks within telomeres could both lead to telomere loss as a result of reduced efficacy of repair processes at these sites[27].

1.5 DYSFUNCTIONAL TELOMERES INITIATE CHROMOSOME INSTABILITY AND DISEASE

The vast majority of malignant tumors exhibit structural and/or numerical chromosome aberrations, with most carcinomas having highly complex and variable cytogenetic changes[275,276]. Genetic variability has been shown not only to differ between tumor cases, but also between cells within the same tumor. In some highly aggressive cancers, heterogeneity is observed in essentially all cells, with only two or three cells amongst those sampled having precisely the same complement of chromosomes[277]. While a small number of tumors has been reported that have intact telomeres and low levels of CIN[277], they appear to be the exception rather than the rule. In contrast, telomere shortening has been reported in a large number of human tumours that carry complex chromosome aberrations[276,278,279]. Abnormally short telomeres have been associated with a wide spectrum of mitotic disturbances. An example of this was observed in a colorectal cancer cell line in which short telomeres were shown to result in an increased frequency of NPBs, whole chromosome lagging and mitotic multi-polarity[278]. Observations such as these have led to the suggestion that loss of telomere integrity may be an early and critical molecular change that leads to initiation, as well as progression, of the oncogenic process[27,276].

CIN arising from dysfunctional telomeres can lead to structural rearrangement of chromosomes, loss of whole chromosomes, and the formation of nucleoplasmic bridges (NPBs) due to end fusions[14,276]. Unprotected telomeres are known to fuse and form chromosomes that are either ring-shaped or dicentric, and dicentric chromosomes can then break unevenly at anaphase if the centromeres are pulled to opposite poles[280]. NPBs arising from dicentric chromosomes can lead to BFB cycles, where breakage leaves chromosome ends unprotected and a cycle of fusions and breakages is established (Figure 1.2). This can result ultimately in gene amplification, altered gene dosage and the compounding effects of increasing CIN[12,33,281,282]. Recent studies in human tumour cells have shown that NPBs can break at multiple sites, leading to loss of DNA fragments or possibly whole chromosome arms[276]. NPBs may also result in mechanical detachment of one or several sister chromatids from the spindle, with the potential for loss of whole chromosomes. Alternatively, the NPBs may lead to the mitotic process being aborted all together[276].

Telomere-based BFB events have been found to coincide with an upsurge in CIN during the process of benign to malignant transition in breast and colorectal cancers[226,283]. Human breast cancers evolve through four defined stages; usual ductal hyperplasia, atypical ductal hyperplasia (ADH), ductal carcinoma *in situ* (DCIS), and invasive and metastatic cancer. A study using FISH to explore genome instability at each of these stages showed that the transition from ADH to DCIS is a critical point at which maximum increases in both NPBs and CIN coincide with critical shortening of telomeres[283]. This finding supported previous evidence showing that there is activation of telomerase at the DCIS stage of breast cancer, while thereafter the level of CIN remained relatively consistent[283]. Further evidence, using a model of immortalised human mammary epithelial cells cultured *in vitro*, showed that telomere-based crisis is pivotal during the oncogenic process in breast cancer. Telomeres were shown to progressively shorten in these cells until passage 22, at which point telomerase was activated. The timing of this again coincided with the highest number of NPBs and the highest level of CIN[283]. Rudolph *et al* (2001) made a similar observation in human colorectal cancer cells[226]. A peak in NPBs was recorded in early high-grade dysplastic lesions, whereas the frequency of NPB was lower in more advanced stages of carcinoma. Telomere shortening occurred during the period of rapid cell proliferation in the early stages of the neoplastic process[226]. The decline in frequency of NPBs, and the point at which telomerase was activated were found to coincide, and beyond this point TL was stable[226]. Taken together, these data support the idea that telomere-based crisis is a crucial event driving genomic instability and disease in the evolution of neoplastic lesions[226,283,284].

1.6 FOLATE DEFICIENCY, DYSFUNCTIONAL TELOMERES AND CHROMOSOME DAMAGE

As discussed earlier, folate-insufficiency results in incorporation of uracil into newly synthesised or repaired DNA in place of thymidine[92,285]. The high thymidine content of telomeric DNA may make this sequence particularly vulnerable to conditions of folate deficiency. When uracil is incorporated into DNA, it is excised and replaced with thymidine, a process requiring both the checkpoint and BER pathways[256]. Where folate is limiting, pools of intracellular thymidine are reduced, and more uracil is likely to be incorporated into the genome, possibly impacting on integrity of the thymidine-rich telomere sequence. As a result, there is potential for multiple transient nicks to be created by uracil glycosylase, together with the action of APE1[92,96]. This may result in greater risk of single and/or double strand breaks in telomeres. Evidence has been presented showing that where two uracils are excised within twelve bases of each other on opposing DNA strands, the frequency of DSBs is increased significantly compared to excision of a single uracil[75]. Thus, it is plausible that folate insufficiency may lead to telomere breakage and loss, telomere shortening and CIN, all of which lay the foundations for a cell that has aberrant nuclear material (Figure 1.7).

The presence of uracil in the genome is recognised to be highly mutagenic. However, under normal cellular conditions the presence of uracil in DNA is an infrequent event, possibly arising from spontaneous deamination of cytosine rather than the incorporation of an incorrect base by DNA polymerases[286]. As discussed above, the frequency of uracil incorporation increases when folate is limiting[92,285]. Furthermore, several folate-sensitive fragile sites have been reported in telomeric sequences, leading to chromosomal aberrations[287]. Taken together with the potential for the telomere position effect (TPE) to inhibit effective checkpoint and DSB repair responses to lesions within telomeric repeats[27,271,272], the impact of low cellular folate on telomere integrity could be considerable.

Another possible effect of increased uracil in telomere repeats is a reduction in telomere capping. Binding assays performed to determine whether oxidative DNA damage in telomeres alters the binding activity of the key shelterin proteins TRF1 and TRF2 showed that one or two 8-oxo-guanine lesions in a defined tract of telomeric DNA reduced the amount of bound protein by 50% compared with undamaged telomeric DNA[139]. Furthermore, multiple lesions (one oxidised guanine per hexamer repeat) reduced bound TRF1/2 to barely detectable levels. Further experiments were conducted to assess whether abasic sites arising from BER affected

binding of TRF1/2[139]. The results demonstrated that the presence of a single AP site in each telomeric repeat decreased binding approximately two fold. The authors concluded that the loss of single or multiple bases within a telomeric tract resulted in disruption of TRF1 and TRF2 interaction and binding with their telomeric substrate. It is plausible, given the specificity of TRF1 and TRF2 for the telomeric sequence, that uracil (or abasic sites due to excision of uracil) in the sequence may alter binding kinetics. Abasic sites arising from uracil excision may also disrupt telomere capping and potentially lead to loss of telomere integrity and formation of end fusions.

It is plausible, therefore, that the high level of CIN observed in PBL cultured in low FA conditions may be due in some part to damage arising from dysfunctional telomeres. MNi may be indicators of chromosome breakage due to uracil incorporation and BER, while NBuds may be indicators of the presence of amplified genes due to BFB cycles. Furthermore, the presence of NPBs may be indicative of fusion events between exposed or uncapped ends of telomeres. As a result of reduced binding by shelterin proteins in the presence of uracil, the integrity of telomere capping may be compromised, again presenting as fusion events between chromosomes. In addition, the exposed ends of chromosomes, in the case of a DSB, may be vulnerable to targeting by NHEJ processing, thus leading to chromosome fusions and BFB cycles.

1.7 KNOWLEDGE GAPS

Based on the evidence discussed above, the following questions were formulated in order to address important gaps in knowledge.

1. Does folate insufficiency cause telomere shortening and chromosome instability?
2. Does uracil incorporation induced by folate insufficiency give rise to accelerated telomere shortening and is this the result of increased frequency of double strand breaks within these structures?
3. Does uracil incorporation into the telomere induced by folate insufficiency result in reduced telomere integrity, thus giving rise to increased chromosome end fusions and nucleoplasmic bridges?

Figure 1.7 A model of strand breakage in telomeres, caused by base excision repair (BER) where uracil (U) is present in telomeric DNA. Folate deficiency causes a high ratio of dUMP:dTMP in the cell, resulting in increased incorporation of U into DNA in place of thymidine. U bases are then excised by uracil glycosylase, leading to abasic sites and double strand breaks (DSB) in DNA. DS breakage occurs if U is present on complementary DNA strands within twelve bases of each other, and an endonuclease (*eg.* APE1) nicks the abasic site during the BER process[96]. In this model, these events may occur after at least two cell divisions and they may be self-perpetuating in conditions of folate deficiency (Adapted from Bull & Fenech, 2008[13]).

CHAPTER 2: AIMS, HYPOTHESES & MODELS

2 AIMS, HYPOTHESES AND MODELS

2.1 AIMS & HYPOTHESES

The main aim of this thesis was to address important knowledge gaps regarding the possible dependency of telomere length maintenance and function on folate status. The project aimed also to study the relationship between telomere length and biomarkers of chromosomal instability under both folate-replete and folate-deficient conditions.

The experiments and investigations tested the following hypotheses:

1. Folic acid (FA) deficiency causes telomere shortening in human cells cultured *in vitro*.
2. Chromosomal instability (CIN) arising from FA deficiency (as determined by frequency of biomarkers MN, NBuds and NPBs) is negatively associated with telomere length in human cells cultured *in vitro.*
3. Lower folate status *in vivo* is associated with shorter telomeres in PBL of healthy adults.

2.2 EXPERIMENTAL MODELS

These hypotheses were tested in WIL2-NS cells and peripheral blood lymphocytes (PBL) by comparing telomere length and degree of CIN in cultures containing low, medium or high concentrations of FA. Several methods are available for measurement of telomere length (qPCR, Q-FISH, Southern blot and flow-FISH). For this study a flow cytometric (flow-FISH) method developed by Lansdorp and colleagues[288,289] was used to determine telomere length in populations of whole cells. This method was selected for its high throughput potential (compared with Q-FISH and Southern blot), the rapid and reproducible nature of the protocol, and for the capacity to exclude dead and dying cells while identifying and isolating cells at the G_0/G_1 phase of the cell cycle with a high degree of specificity. CIN was determined using the Cytokinesis-Block Micronucleus Cytome (CBMN Cytome)[14] assay to compare frequencies of binucleated cells containing MN, NBuds and NPBs. Cytostasis was determined by comparing the ratios of mono-, bi-, and multinucleated cells, while percentages of necrotic and/or apoptotic cells were measured to assess the cytotoxic effects of treatments.

WIL2-NS is a human B lymphoblastoid cell line with a deficiency in apoptotic response due to a p53 mutation that allows cells with chromosomal damage to survive. This feature, together with clearly defined cellular and nuclear morphology, make WIL2-NS cells ideal for measuring induction of DNA damage as cells with chromosomal damage are not eliminated via apoptosis. While telomere dynamics of the WIL2-NS cell line have not been studied previously, earlier studies conducted in this laboratory have shown that the WIL2-NS cell line is a sensitive and accurate model for determining chromosomal damage[36,95,290].

PBL were also selected as a model for these preliminary studies on the effects of FA on telomere length. PBL are readily accessed from venous blood samples and they provide an excellent model for *in vitro* studies, as well as comparative *in vivo* investigations. In particular, the T cell component can be activated by exposure to polyclonal mitogens such as phytohaemagglutinin (PHA) or concanavalin A (Con A) under controllable conditions. The majority of primary lymphocytes are in the G_0 stage of the cell cycle and as cells in G_0 tend to have lower repair activity than cycling cells, this provides an opportunity to investigate accumulated DNA lesions[291]. Thus, these long-lived cells provide an ideal system for measuring and analysing lesions accumulated over extended periods of nutrient deficiency

To test the relationship between telomere length and folate status *in vivo*, 43 young (18-32 years) and 47 older (65-83 years) adults were recruited to provide a single blood sample. Telomere length was determined on PBL using the flow cytometric assay. qPCR hydrolysis probe allelic discrimination was used to determine the genotypes of donors with respect to common polymorphisms in genes involved in folate metabolism genes: *methylene-tetrahydrofolate reductase* (*MTHFR C677T*) and *methionine synthase* (*MTR A2756G*). This was performed to test for effects of these common single nucleotide polymorphisms (SNPs), which are known to affect folate metabolism *in vitro* and *in vivo*. Levels of plasma folate, red cell folate, plasma vitamin B12 and plasma homocysteine were analysed to examine possible relationships with telomere length in PBL, taking into account also age, gender, BMI and genotype.

CHAPTER 3: MATERIALS & METHODS

3 MATERIALS AND METHODS

3.1 CELLS

3.1.1 WIL2-NS human cell line

WIL2-NS is a human non-immunoglobulin-secreting B lymphoblastoid cell line, originally obtained from the spleen of a 5-year-old Caucasian male who was suffering from hereditary spherocytic anaemia[292], for which standard treatment includes splenectomy. WIL2-NS cells have a G-A transition mutation in codon 237 of the p53 gene, resulting in replacement of methionine by isoleucine[293]. This mutation of the p53 gene product causes a reduction in the apoptotic response to radiation[294,295]. The suppressed apoptotic activity allows cells with chromosomal damage to survive, and this feature, together with clearly defined cellular and nuclear morphology, makes the WIL2-NS cell line ideal for measuring DNA damage using the cytokinesis-block micronucleus (CBMN) Cytome assay because cells with chromosomal damage are not eliminated via apoptosis. The cells were sourced from the American Type Culture Collection (CRL-8155) (ATCC, USA).

3.1.2 Fresh lymphocytes

3.1.2.1 Blood collection

Trained nursing staff at the CSIRO Human Nutrition Clinical Research Unit collected blood by venepuncture from overnight-fasted adult volunteers, with written consent. Blood samples were collected into 8ml LiHep tubes and stored at room temperature (RT) prior to preparation of mononuclear cells.

3.1.2.2 Isolation of mononuclear cells from whole blood

Blood was transferred to a sterile 70ml container (Technoplas, Australia) and diluted 1:1 with sterile HBSS (Thermo Electron, Melbourne, Australia) at RT. The diluted blood was gently layered over the top of Ficoll-paque^{TM} Plus (Pharmacia Biotech, Uppsala, Sweden) in a sterile polystyrene conical base 50ml tube (50ml Falcon tube) (Becton Dickinson, NJ, USA) at a ratio of 1:3 (Ficoll:diluted blood). The tubes were centrifuged at 400rpm at 18°C for 30 minutes (Rotanta 460R, Hettich, Germany). Cells at the interface between the two upper layers were removed in approximately 5-8ml using a sterile glass Pasteur-pipette, taking care not to disturb the surrounding layers. The cells were transferred to a sterile conical 50ml tube and HBSS (at

RT) was added (1:3; cell suspension:HBSS), mixed well and centrifuged at 180rpm for 10 minutes at RT. The pellet was resuspended in a further 10ml of HBSS and centrifuged at 100rpm for 10 minutes. The pellet of cells was then resuspended in 1ml of PBS or an appropriate culture medium. All steps were performed in a biohazard fume cupboard to ensure protection of the sample and the operator. Cells were then counted using a Coulter Counter (refer 3.2.2 below).

3.1.3 1301 human cell line

1301 cells are a human lymphoblastoid cell line derived from a T-cell leukemia[296,297] and were sourced from the European Collection of Cell Cultures, (accession number 01051619). These cells were used as a reference for measurement of telomere length by flow cytometry, because of their high telomere content. 1301 cells are reported to have telomeres up to 80kb in length[297].

3.2 TISSUE CULTURE

3.2.1 Media reagents and preparation

3.2.1.1 Complete medium and tissue culture conditions for growth of the WIL2-NS cell line

Cells were grown and maintained in complete medium, consisting of RPMI 1640 (R0883, Sigma, Australia) supplemented with 5% (v/v) heat inactivated foetal bovine serum (HI-FBS) (Thermo Trace, Australia), 1% (v/v) penicillin [5000IU/ml]/streptomycin [5mg/ml] (Sigma, Australia) and 2mM L-glutamine (Sigma, Australia). Flasks were placed horizontally with lids loosened in a 5% carbon dioxide humidified incubator at 37°C (Quantum Scientific, Brisbane, Australia).

3.2.1.2 Complete medium and tissue culture conditions for fresh lymphocytes

Fresh lymphocytes were isolated from whole blood and placed in complete medium comprising RPMI 1640 (R0883, Sigma, Australia) supplemented with 10% (v/v) foetal bovine serum (FBS) (Thermo Trace, Australia), 5% interleukin-2 (IL2) [200U/ml] (Roche Diagnostics, Australia), 1% (v/v) penicillin/streptomycin (Sigma, Australia), 2mM L-glutamine (Sigma, Australia) and 1% sodium pyruvate [100mM] (Thermo Trace, Australia). Aliquots of 40ml containing 0.5 x 10^6 cells/ml were placed in 75cm^2 flasks and

phytohaemagglutinin (PHA) [22.5mg/ml] (Oxoid, Australia) was added at a rate of 1.3µl per millilitre of medium to activate T cells. The flasks were incubated vertically, with lids loosened, in a 5% carbon dioxide humidified incubator at a constant temperature of 37°C (Quantum Scientific, Brisbane, Australia). Cultures were split every 3-4 days, using fresh medium supplemented with 5% conditioned (spent) medium as a source of growth factors.

3.2.1.3 Complete medium and tissue culture conditions for growth of the 1301 cell line

Cells were grown in complete medium consisting of RPMI 1640 (R0883, Sigma, Australia) supplemented with 10% (v/v) foetal bovine serum (FBS) (Thermo Trace, Australia), 1% (v/v) penicillin/streptomycin (Sigma, Australia) and 2mM L-glutamine (Sigma, Australia). Flasks were placed horizontally with lids loosened, in a 5% carbon dioxide humidified incubator at a constant temperature of 37°C (Quantum Scientific, Brisbane, Australia). To ensure consistency and to minimise intra-experimental variation, 1301 cells were grown in a large culture and cryopreserved in batches for storage in liquid nitrogen (Chapter 3.2.4) Batches were then thawed as required on experimental days (Chapter 3.2.5).

3.2.1.4 Preparation of folic acid deficient medium

Folic acid (FA)-deficient medium, for experiments using both WIL2-NS and fresh lymphocytes, was prepared using the formulation for complete medium detailed above, with the exception that a percentage of FA-replete RPMI (R0883) was substituted with FA-deficient RPMI (FDM, R1145, Sigma, Australia) to produce desired concentrations of FA. To prepare FDM, the 10x stock was diluted 1:10 with sterile milli-Q water and $NaHCO_3$ (Sigma, Australia) was added as a sterile solution to a final concentration of 2mg/L.

The FA concentration of complete medium prepared using RPMI (R0883) was measured and found to be 3000nM. Accordingly, to achieve a final concentration of FA for experiments using FA-deficient conditions, FA-replete medium was diluted with FA-deficient medium. For example to achieve 300nM FA, one part of RPMI (R0883) was diluted with 9 parts of FDM. After preparation, each batch of medium was stored in sealed sterile bottles at 4°C while FA concentration was tested, and minor adjustments were made where necessary to achieve the specified FA level. FA concentrations were measured by the Department of Chemical Pathology, Institute of Medical and Veterinary Sciences (IMVS) (detail provided in chapter 3.7). Aliquots (99ml) of medium were stored frozen in sterile containers (Technoplas, Australia) at -20°C until required. Vials were then thawed at 4°C and 1ml (1%) of fresh L-Glutamine was added to each vial.

3.2.2 Cell enumeration by Coulter Counter

Cells were enumerated using a Coulter Counter (ZI Coulter® Particle Counter, Beckman Coulter, USA). 30µl of the cell suspension was removed into a standard 20ml vial (accuvette) containing 15ml of Isoton®II solution (1:500 dilution) (Coulter Electronics, NSW, Australia). In the case of freshly isolated lymphocytes, five drops of Zapoglobin®II Lytic Reagent (Coulter Electronics, NSW, Australia) was added to lyse red blood cells (RBC). The diluted sample was analysed according to manufacturer's instructions. Control readings (Isoton II only) were taken in triplicate to ensure a baseline value below 50, and each sample was analysed in triplicate. Cell concentration was calculated from the mean of the three readings, multiplied by 1000 to adjust for the dilution factor and the volume taken up by the counter (0.5ml).

3.2.3 Estimation of cell viability by Trypan Blue exclusion

Aliquots of cell suspensions in either PBS or medium were mixed with sterile filtered trypan blue (TB) (0.4% w/v) (Sigma, Australia) in a 1.5ml microtube. To ensure adequate separation of cells for counting, the ratio of dye to cell suspension was 1:5. Cells were incubated with TB at RT for 5 minutes prior to counting in a haemocytometer (Improved Neubauer, UK), using X40 objective. A percentage of viable cells was calculated based on a minimum of 250 cells (viable and non-viable) scored for each chamber. Viability testing was carried out in duplicate chambers for each sample, and a mean percentage of viable cells calculated. All steps prior to scoring were undertaken in a biological safety cabinet Class II.

3.2.4 Long term cell storage in liquid nitrogen

Following enumeration, cells were aliquotted into a 15ml sterile conical tube (15ml Falcon tube) (Becton Dickinson, "Falcon", NJ, USA), centrifuged at 180g for 10 minutes and resuspended in 900µl sterile FBS. They were then mixed well with 100µl (10%) of sterile DMSO in a 1.8ml Nunc CryoTube^{TM} (Roskilde, Denmark). The cryo-vials were immediately placed in a thick-walled polystyrene box packaged with cotton wool and stored at -80°C for 24 hours, and then transferred to liquid nitrogen storage (RS Series) (Taylor-Wharton, AL, USA). A maximum of 20 x 10^6 viable cells were stored per vial, depending on the cell type and future usage. Viability for freshly isolated lymphocytes was 98-100% prior to freezing. Viability for WIL2-NS cells was tested prior to freezing to ensure accuracy of the numbers of viable cells aliquotted.

3.2.5 Thawing cells from liquid nitrogen storage

Cryo-vials were removed from liquid nitrogen storage and placed immediately into water warmed to 37°C. Cells were thawed by gently agitating the vial in the water, taking care not to immerse the lid. Once thawed, the vial was swabbed with 70% ethanol and the cells were transferred to a 15ml tube containing 10ml PBS at RT. After centrifugation at 180g for 10 minutes, the cells were resuspended in a further 10ml PBS, and centrifugation repeated. The pellet was then resuspended in 1ml of either medium or PBS, cells were counted and an estimate of viability was made. The cells were then grown in complete medium for 5-7 days, prior to being split into treatment medium at for the commencement (day 0) of each experiment.

3.3 CYTOKINESIS-BLOCK MICRONUCLEUS (CBMN) CYTOME ASSAY

3.3.1 Overview

The cytokinesis-block micronucleus (CBMN) cytome assay is a comprehensive system for measuring DNA damage, cytostasis and cytotoxicity[14]. Markers of DNA damage are scored specifically in once-divided binucleated (BN) cells and include (a) micronuclei (MNi), a biomarker of chromosome breakage and/or whole chromosome loss; (b) nucleoplasmic bridges (NPBs), a biomarker of DNA misrepair and/or telomere end-fusions; and (c) nuclear buds (NBUDs), a biomarker of elimination of amplified DNA and/or DNA repair complexes[14] (Figure 3.1). Nuclear division index (NDI) can be calculated by measuring the proportion of apoptotic, necrotic, mono-, bi-, and multinucleated cells. The CBMN Cytome assay is widely used to assess the genotoxic or protective effects of pharmaceuticals, dietary nutrients, chemical and radiation exposure, both *in vivo* and *in vitro*, and has been shown to be a sensitive predictor of cancer risk [14,22].

The assay involves culturing dividing cells *in vitro* in the presence of cytochalasin-B (Cyto-B) to inhibit actin polymerisation and thus the formation of the cleavage furrow at cytokinesis. As a result, dividing cells are blocked at the binucleate stage, providing an opportunity for damage, such as NPBs, to be directly observed. It is essential that nuclear division is completed, to allow the expression of biomarkers scored in the CBMN Cytome assay (MNi, NPBs and NBuds) but cytokinesis is prevented, so that NPBs are not broken. Following Cyto-B treatment, cells are harvested onto slides by cytocentrifugation and stained to differentiate cytoplasm from nuclear material. Chromosomal damage markers are then scored by light microscopy. The standard protocol involves scoring damage in 1000 BNed cells per slide, on duplicate slides.

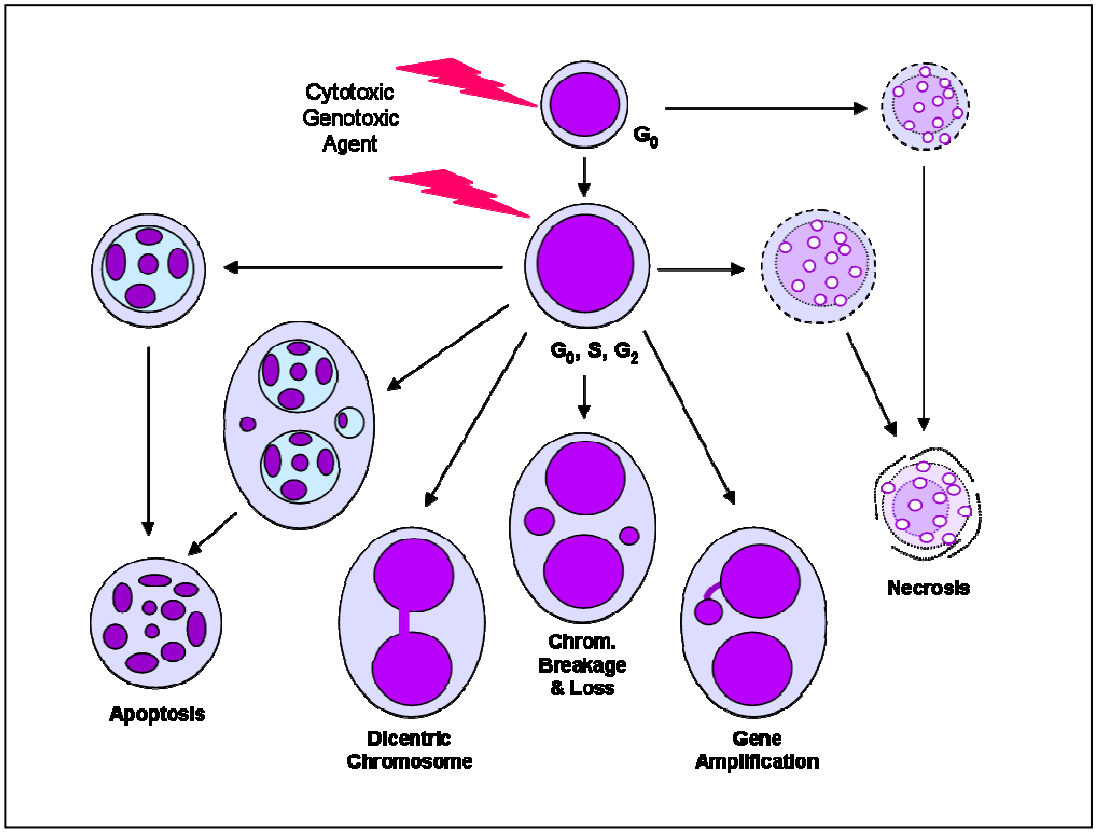

Figure 3.1 The various possible fates of cultured cells in which cytokinesis was blocked following exposure to cytotoxic/genotoxic agents. Using the morphological biomarkers that can be observed by microscopy in the Cytokinesis-block Micronucleus Cytome (CBMN-Cyt) assay, it is possible to measure: the frequency of nucleoplasmic bridges (NPB), a biomarker of asymmetrical chromosome rearrangements that result in dicentric chromosomes due to misrepair of chromosome breaks or telomere end fusions; micronuclei (MNi), a biomarker of chromosome breakage or loss; nuclear buds (NBuds), a biomarker of gene amplification; apoptosis and necrosis. (Adapted from Fenech *et al*, 2003[22,23])

3.3.2 Lymphocyte culture and addition of Cytochalasin-B

3.3.2.1 Preparation of Cytochalasin-B stock and working solutions

The vial containing 5 mg of Cytochalasin B (Cyto-B) (Sigma, Australia) was removed from storage at -20°C and allowed to equilibrate to RT. The top of the rubber seal was sterilised with 70% ethanol, the ethanol was allowed to evaporate and the seal was vented with a 25G needle attached to a 0.2µm hydrophobic filter to break the vacuum. 8.33ml of sterile DMSO was transferred to a sterile 50ml Falcon tube and 4ml of this was then transferred through the seal and using a 5ml sterile syringe and mixed gently with the onto the Cyto-B. The solution was removed and transferred to a separate, sterile tube. This was repeated using the remaining 4.33ml of DMSO, to create a final volume of 8.33ml of 600µg/ml stock solution. 100µl volumes of the latter were then aliquotted into labelled 5ml polystyrene tubes and stored at -20°C for up to 12 months. Prior to addition into culture, 900µl of pre-warmed treatment medium was added to each thawed aliquot, to obtain 1000µl of working solution at 60µg/ml. All steps were performed in a cyto-guard cabinet, with personal protective clothing worn throughout (Tyvek gown, P2 dust mask, double nitrile gloves and safety glasses).

3.3.2.2 Preparation of phytohaemagglutinin (PHA) stock solution

To prepare the 10x stock solution, 2ml of sterile isotonic saline was added to a vial containing 5 mg of phyohaemagglutinin (PHA) (Oxoid, Australia), forming a solution of 2.5mg/ml. 200µl volumes of the solution were aliquotted into labelled 5ml polystyrene yellow capped tubes and stored at -20°C for up to 1 month.

3.3.2.3 Establishment of WIL2-NS cultures for CBMN Cytome Assay

Cells were maintained in complete or treatment medium (as per Chapters 3.2.1.1) for the duration of each experiment. At each sample day within each experiment an aliquot of cells was removed from culture, centrifuged and resuspended in 1ml of the appropriate treatment medium (as per 3.2.1.4). Cells were then counted (as per Chapter 3.2.2) and viability tested (Chapter 3.2.3) to obtain the viable cell concentration. Four 500µl cultures per treatment were then established in a sterile 24 well flat-bottomed tissue culture plate (Corning, NY, USA). This procedure is summarised at Figure 3.2.

A final concentration of 0.3×10^6 viable cells per culture was achieved using the following calculation:

$$\frac{\text{Target cell concentration } (0.3 \times 10^6)}{\text{Viable cell concentration of sample cells}} \times 500 = x \text{ µl of sample cell suspension}$$

The calculated volume of cell suspension was added to the wells and the balance of each 500µl culture was made up with the relevant treatment medium warmed to 37°C. For example, if the viable cell concentration of sample cells was 5.8×10^6/ml the following would apply:

$$\frac{0.3 \times 10^6}{5.8 \times 10^6} \times 500 = 25.9\text{µl of sample cell suspension per culture well}$$

474.1µl of medium was then added to make the culture up to a final volume of 500µl per well.

The culture plates were shaken gently prior to placing in a CO_2 incubator (5% CO_2, 37°C) and "Time 0" was recorded. Following 2 hours incubation ("Time 2hr"), 37.5µl of 60µg/ml Cyto-B was added to each culture, achieving a final Cyto-B concentration of 4.5µg/ml. Plates were shaken gently to mix well and returned to the incubator for a further 22 hours.

Cells were then harvested by cytocentrifugation onto glass microscope slides at "Time 24hr" (refer Chapter 3.3.3 below) (Figure 3.2).

Following page:

Figure 3.2 Overview of the Cytokinesis-block Micronucleus Cytome (CBMN-Cyt) Assay. (A) Cells are maintained in culture in treatment medium. (B) At each sample point, aliquots of cells are removed from culture, centrifuged and resuspended in 1ml of the appropriate treatment medium. Cell counts and viability assessments are conducted. (C) 500µl cultures are then established in a 24-well microplate (n = 4 cultures per treatment). After a 2-hour incubation, cytochalasin-B is added to each well to block dividing cells at the binucleate stage. This is followed by a further 22-26 hour incubation (depending on cell type). (D) Cells are then harvested onto glass microscope slides by cyto-centrifugation, stained with Diffquick, and scored using light microscopy. (E) An example of the timing of Cyto-B addition, and harvest, for each of the sample points over a 21-day study in WIL2-NS cells, where samples were obtained every 7 days for measurement of DNA damage biomarkers.

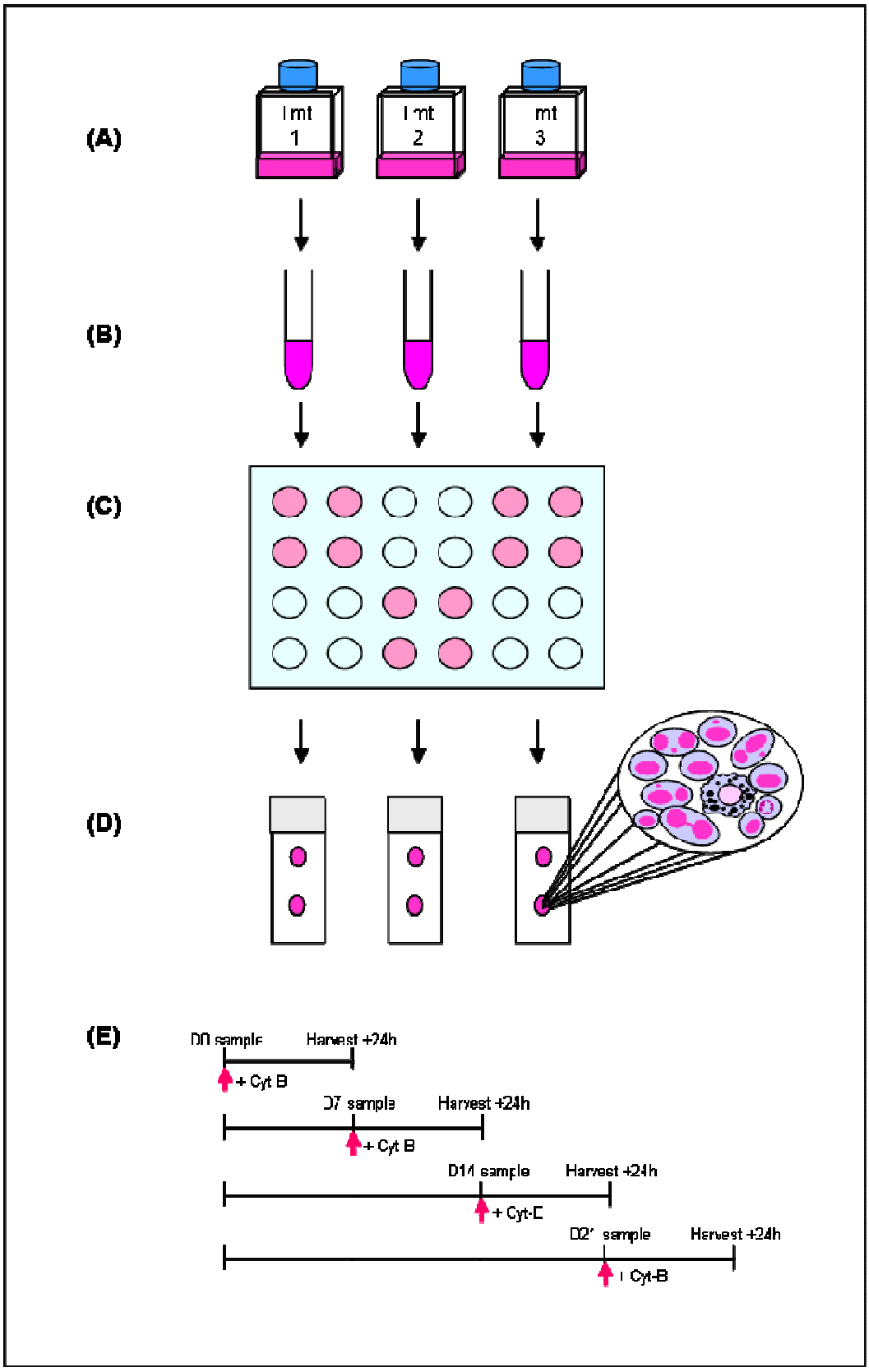
(A)
mt 1
mt 2
mt 3
(B)
(C)
(D)
(E)
D0 sample
Harvest +24h
+ Cyt B
D7 sample
Harvest +24h
+ Cyt B
D14 sample
Harvest +24h
+ Cyt-B
D21 sample
Harvest +24h
+ Cyt-B

3.3.2.4 Establishment of fresh lymphocyte cultures for CBMN Cytome Assay

Isolated lymphocytes were maintained in complete or treatment medium (as per Chapters 3.2.1.2) for the duration of each experiment. At each sample day within each experiment an aliquot of cells was removed from culture, centrifuged and resuspended in 1ml of the appropriate treatment medium (as per 3.2.1.4). Cells were then counted (Chapter 3.2.2) and tested for viability (Chapter 3.2.3) to obtain the viable cell concentration. Eight 500µl cultures per time point, per treatment, were then established in a sterile 24 well flat-bottomed tissue culture plate (Corning, NY, USA). This procedure is summarised at Figure 3.2.

A final concentration of 0.5 x 10^6 viable cells per culture was achieved using the following calculation:

$$\frac{\text{Target cell concentration } (0.5 \times 10^6)}{\text{Viable cell concentration of sample cells}} \times 500 = x \text{ µl of sample cell suspension}$$

The calculated volume of cell suspension was added to the wells and the balance of the 500µl culture was made up with the relevant treatment medium, warmed to 37°C. For example, where the viable cell concentration was 5.8 x 10^6/ml:

$$\frac{0.5 \times 10^6}{5.8 \times 10^6} \times 500 = 43.1\text{µl of sample cell suspension per culture well}$$

456.9µl of medium was then used to make each culture up to a final volume of 500µl per well.

Plates were shaken gently and placed in a CO_2 incubator (5% CO_2, 37°C) and "Time 0" recorded. Following 2 hours incubation ("Time 2hr"), plates were removed and 37.5µl of 60µg/ml Cyto B was added to each culture, achieving a final Cyto B concentration of 4.5µg/ml. Plates were shaken gently to mix well and then returned to the incubator for a further 24 hours. Cells were then harvested onto slides at "Time 26hr" (refer Chapter 3.3.3 below).

3.3.3 Cell harvest and staining

Glass microscope slides (Knittel Gläser, Germany) were washed in absolute ethanol, dried and labelled. They were then assembled in a slide holder with a filter card (Thermo Electron, Melbourne, Australia) and cytocentrifuge cup, arranged in the cytocentrifuge (Shandon Scientific Limited, UK) rotor and numbered 1-12. Cells in each culture well were resuspended gently, and a 120µl sample was transferred into the cup of the corresponding numbered slide in the rotor. After centrifugation for 5 minutes at 600rpm at RT, the slides were carefully rotated and the process repeated to create a duplicate spot on each slide. Each slide holder was then carefully dismantled and the slides were placed in a rack to dry for exactly 10 minutes prior to fixing for 10 minutes in methanol. The slide rack was then transferred to Diff-Quik solution 1 (orange) (Diff-Quik Kit, Lab Aids, Australia) and stained for 6 seconds, while moving the rack back and forth, and then into Diff-Quik solution 2 (blue) for another 6 seconds. The slides were then washed gently under running RO water, excess water was removed by flicking, and they were allowed to air dry. Each slide was checked by microscopy prior to coverslipping to ensure an even coverage of cells and appropriate staining. When thoroughly dry, slides were coverslipped in a fume hood using DePex (Merck, Germany) and then left overnight in the fumehood to dry, prior to scoring.

3.3.4 Slide scoring method

At the end of each experiment, two slides from each time point in each treatment were randomly numbered and coded by an independent operator prior to scoring by the "blinded" experimenter. Slides were only un-blinded when all slides for an individual experiment had been scored. Slides were scored under 1000x magnification (10x objective, 100x oil immersion lens), using a conventional light microscope (Leica). Initially, all cells on the slide were scored in the categories of apoptotic, necrotic, mono-, bi- and multi-nucleated, until a total of 500 cells was reached, providing data to calculate the nuclear division index (NDI). From this point onwards, only binucleated (BN) cells were scored until a total of 1000 BN was achieved. Chromosomal damage biomarkers (MNi, NBuds and NPBs) were only recorded when they occurred in a BN cell. An example of a scoring sheet is provided at Figure 3.3.

3.3.5 Calculation of the nuclear division index (NDI)

The NDI provides a measure of the proliferative status of the viable cell fraction[14]. NDI at each time point and for each culture condition was calculated, using the proportions of mono-, bi- and multinucleated cells, to give an estimate of the cell division frequency. NDI is calculated according to a modified form of the equation proposed by Eastmond and Tucker[298]:

NDI = {(M1 + (2 x M2) + (3 x M3)) / N}, where M1 and M2 represent the number of cells with one or two nuclei respectively, M3 represents all multinucleated cells (*ie.* >2 nuclei per cell) and N is the total number of viable cells scored.

3.3.6 Cell scoring criteria

Cell types and chromosomal damage markers were scored according to the criteria proposed by Fenech (2007) and detailed below[14].

3.3.6.1 Criteria for scoring viable mono-, bi- and multinucleated cells

- Mono-, bi- and multinucleated cells are those with an intact cytoplasm and normal nuclear morphology, containing one, two and three or more nuclei, respectively (Figure 3.4).
- These cells may or may not contain MNi, NBuds and in the case of bi- and multinucleated cells they may or may not contain one or more NPBs (Figure 3.5)[14].

3.3.6.2 Criteria for scoring BN cells suitable for scoring markers of chromosomal damage

The cytokinesis-blocked BN cells that may be scored for MN, NPB and NBud frequency should have the following characteristics (Figure 3.4B):

- The cells should be binucleated (BN).
- The two nuclei in a BN cell should have intact nuclear membranes and be situated within the same cytoplasmic boundary.
- The two nuclei in a BN cell should be approximately equal in size, staining pattern and staining intensity.
- The two nuclei within a BN cell may be attached by a NPB, which is no wider than 1/4th of the nuclear diameter.
- The two main nuclei in a BN cell may touch but ideally should not overlap each other. A cell with two overlapping nuclei can be scored only if the nuclear boundaries of each nucleus are distinguishable.
- The cytoplasmic boundary or membrane of a BN cell should be intact and clearly distinguishable from the cytoplasmic boundary of adjacent cells[14].

3.3.6.3 Criteria for scoring apoptotic cells

Apoptotic lymphocytes are cells undergoing programmed cell death. They have the following characteristics:

- Early apoptotic cells can be identified by the presence of chromatin condensation within the nucleus and intact cytoplasmic and nuclear membranes (Figure 3.4E)

- Late apoptotic cells exhibit nuclear fragmentation into smaller nuclear bodies within an intact cytoplasm/cytoplasmic membrane (Figure 3.4F).
- Staining intensity of the nucleus, nuclear fragments and cytoplasm in both early and late stage apoptotic cells is usually greater than that of viable cells[14].

3.3.6.4 Criteria for scoring necrotic cells

Necrosis is an alternative form of cell death that is thought to be caused by damage to cellular membranes, organelles and/or critical metabolic pathways required for cell survival such as energy metabolism. Necrotic lymphocytes have the following characteristics (Figure 3.4D):

- Early stage necrotic cells have a pale cytoplasm, the presence of numerous vacuoles (mainly in the cytoplasm and sometimes in the nucleus), damaged cytoplasmic membrane and a fairly intact nucleus.
- Late stage necrotic cells exhibit loss of cytoplasm and damaged/irregular nuclear membrane, with only a partially intact nuclear structure and often with nuclear material leaking from the nuclear boundary.
- Staining intensity of the nucleus and cytoplasm in both types is usually less than that of viable cells[14].

3.3.6.5 Criteria for scoring Micronuclei (MNi)

Micronuclei represent chromosome fragments or whole chromosomes that lag behind at anaphase during nuclear division. They are morphologically identical to, but smaller than, nuclei. They have the following characteristics (Figure 3.5A,B)[14]:

- The diameter of MNi in human lymphocytes usually varies between $1/16^{th}$ and $1/3^{rd}$ of the mean diameter of the main nuclei, which corresponds to $1/256^{th}$ and $1/9^{th}$ of the area of one of the main nuclei in a BN cell, respectively.
- MNi are non-refractile and they can therefore be readily distinguished from artefact such as staining particles.
- MNi are not linked or connected to the main nuclei.
- MNi may touch but not overlap the main nuclei and the micronuclear boundary should be distinguishable from the nuclear boundary.
- MNi usually have the same staining intensity as the main nuclei but occasionally staining may be more intense.

3.3.6.6 Criteria for scoring Nucleoplasmic bridges (NPBs)

An NPB is a continuous DNA-containing structure linking the nuclei in a BN cell. NPBs originate from dicentric chromosomes (resulting from mis-repaired DNA breaks or telomere end fusions) in which the centromeres are pulled to opposite poles during anaphase. They have the following characteristics (Figure 3.5C)[14]:

- The width of an NPB may vary considerably but usually does not exceed 1/4th of the diameter of the nuclei within the cell.
- NPBs should also have the same staining characteristics as the main nuclei.
- On rare occasions more than one NPB may be observed within one BN cell (Figure 3.5D).
- A BN cell with one or more NPB may also contain one or more MNi (Figure 3.5E).

Due to the importance of NPBs with respect to telomeres, additional criteria were developed to score BN cells with multiple NPBs, and cells where multiple NPB had caused the nuclear morphology of the BN cell to differ from those detailed in the standard scoring criteria above. When the scoring protocol deviated from the standard criteria specified here, detail has been provided within the relevant chapters.

3.3.6.7 Criteria for scoring Nuclear buds (NBuds)

An NBud represents the mechanism by which a nucleus eliminates amplified DNA and DNA repair complexes. They have the following characteristics (Figure 3.5F)[14]:

- Similar in appearance to MNi with the exception that they are connected with the nucleus via a bridge that can be slightly narrower than the diameter of the bud, or by a much thinner bridge, depending on the stage of the extrusion process.
- Usually have the same staining intensity as MNi.
- Occasionally NBuds may appear to be located within a vacuole adjacent to the nucleus.

Following page:

Figure 3.3 Example of scoring sheet used for CBMN Cytome assay

(note: detail regarding BN cells with 'chewing gum' morphology is provided in Chapters 5, 6 and 7)

CBMN Assay Score Sheet amended for telomere assessment & detailed NPB scoring

Score 2 slides, 1000BN per slide

1st 500: Score all cells (mono, BN, Multi, apop, necro and all damage markers) to determine NDI

Continuation: Score binucleated cells only and all of the damage markers (**up to total of 1000 BN**)

NPBs: should be no wider than 1/3 of the nucleus diameter, must be joined at both ends. Broken bridges can not be counted. Where NPBs are clearly discernible record the total number in each cell. Where there are too many to count and/or individual NPBs are not clearly defined (chewing gum effect) these are scored as 5 NPB.

Slide Code #	Uncoded slide label	**Cytostatic / Cytoxicity score**					NDI	NDCI	Total # cells scored (A-E)	**MN and buds in BNs**				**NPBs in BNs**				
		Mono	BN	Multi	Apopt	Necro				#BNs scored	#BNs with MNi	Total #MN in BNs	#BNs with Nbud	1 NPB	2 NPB	3 NPB	4 NPB	Chewing gum (5)
		A	B	C	D	E												
1																		
2																		
3																		
4																		
5																		
6																		
7																		
8																		
9																		
10																		
11																		
12																		
13																		
14																		
15																		
16																		
17																		
18																		
19																		
20																		

NDI: nuclear division index, NDCI: nuclear division cytotoxicity index

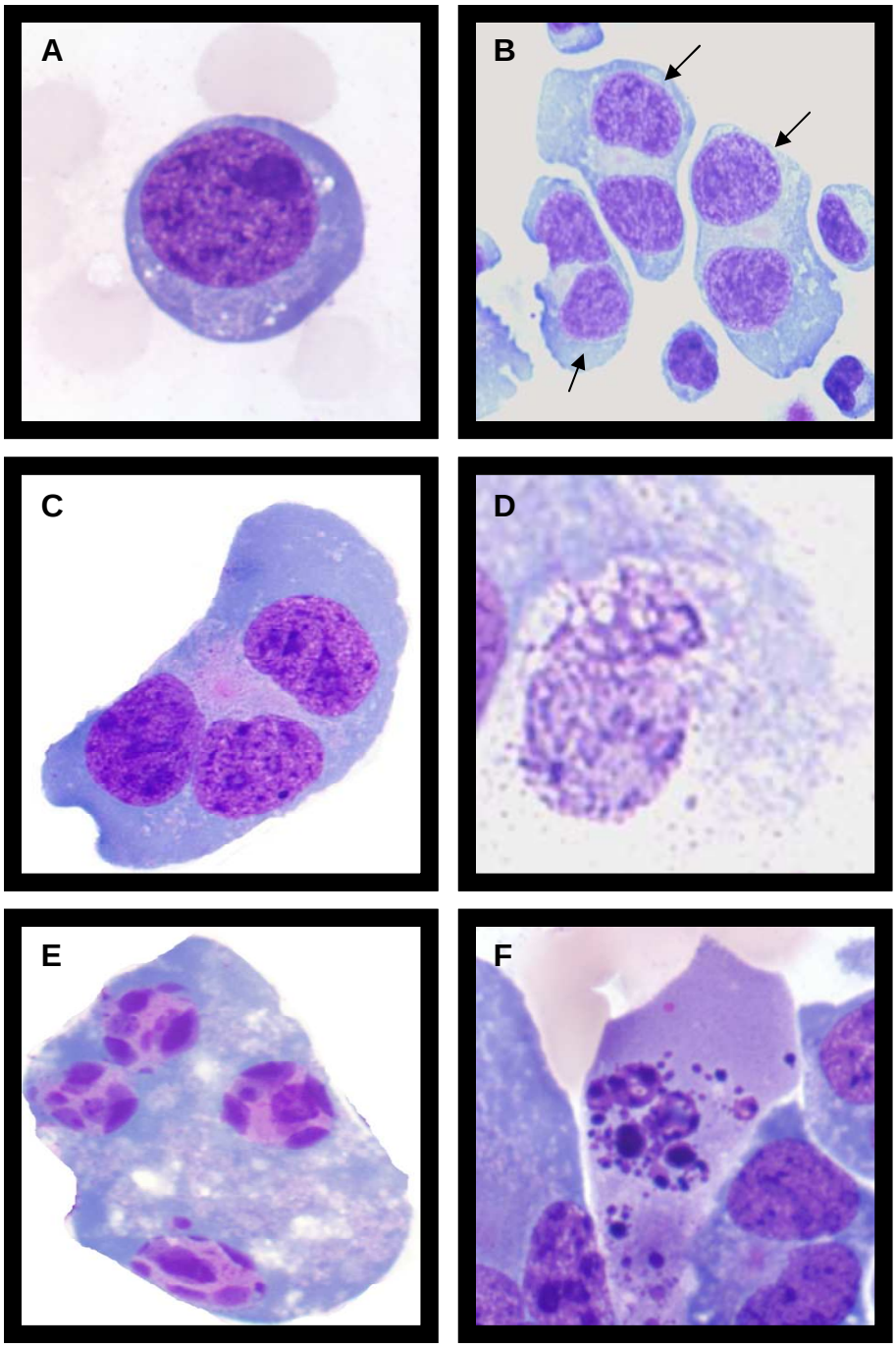

Figure 3.4 Examples of morphological characteristics used to score cells in the Cytokinesis-block Micronucleus Cytome (CBMN-Cyt) Assay. (A) mononucleated cell; (B) binucleated cells; (C) multinucleated cell; (D) necrotic cell; (E) early apoptotic cell; and (F) late apoptotic cell (1000x magnification). (*Photographs by Carolyn Salisbury & Theodora Teo*).

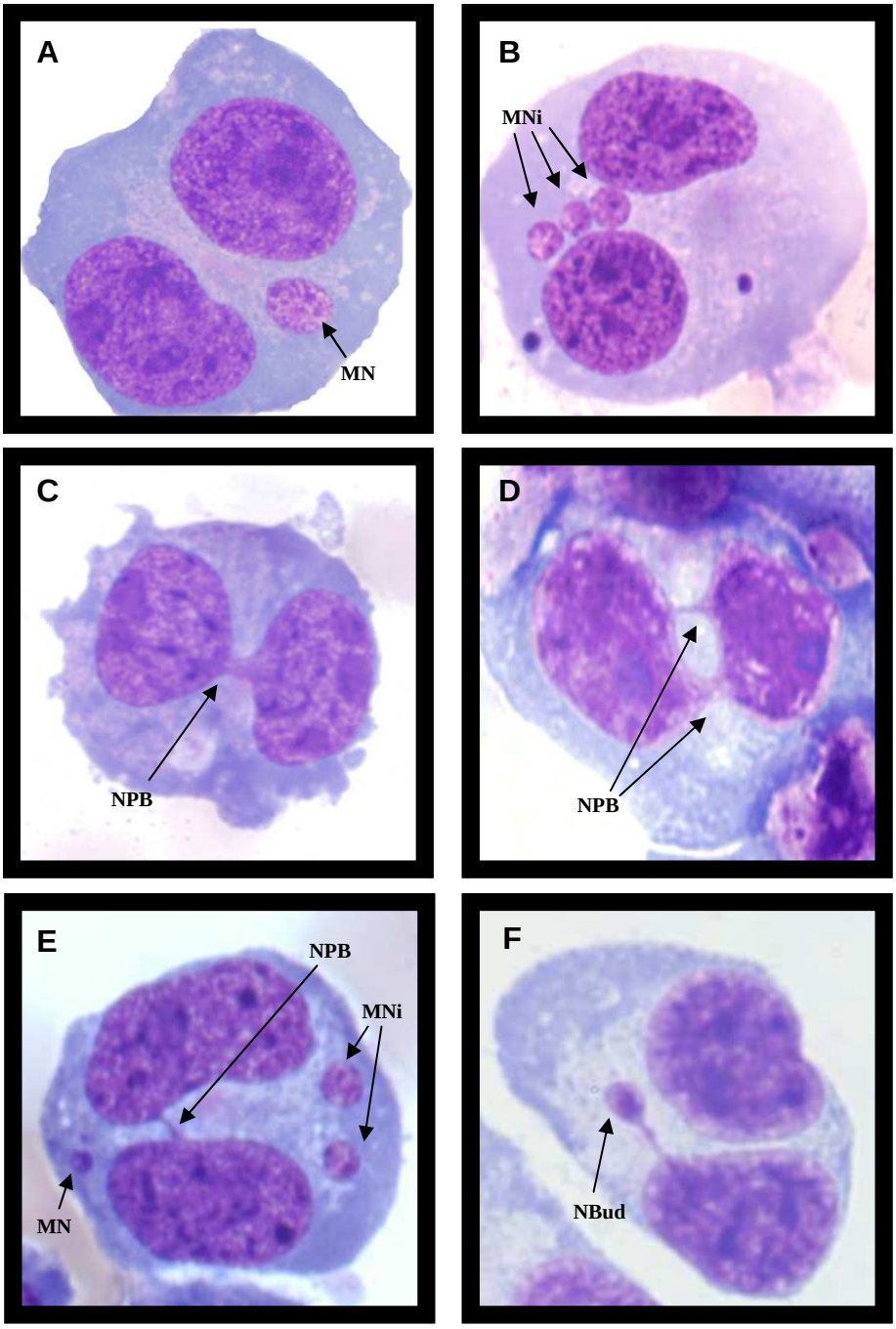

Figure 3.5 Biomarkers of chromosomal damage in cultured cells in which cytokinesis was blocked following exposure to cytotoxic/genotoxic agents in the CBMN-Cyt assay. Using these biomarkers, it is possible to measure the frequency of (A, B) chromosome breakage or loss indicated by presence of one or more micronuclei (MNi); (C, D) chromosome rearrangement (for example, dicentric chromosomes) resulting in one or more nucleoplasmic bridges (NPB); (E) chromosome breakage and end fusion, forming a dicentric chromosome (NPB) and one or more acentric fragments (MNi); and (F) gene amplification, indicated by the presence of nuclear buds (NBuds) (1000x magnification).

3.4 MEASUREMENT OF TELOMERE LENGTH BY FLOW CYTOMETRY

3.4.1 Overview

Telomere length (TL) is conventionally measured using the Southern blot method, and while reproducible, this assay is labour-intensive, requires a large amount of DNA and is subject to inaccuracy by incorporation of subtelomeric DNA[299]. An alternative method of measuring TL, using flow cytometry, was developed by Rufer et al in the Lansdorp laboratory in 1998. It enables measurement of TL to be performed rapidly, accurately, reproducibly and with a high degree of sensitivity to small changes[288]. Furthermore, results are recorded in the form of a frequency distribution of TL in individual cells. Results of TL measured by flow cytometry correlated strongly with the results obtained by the Southern blot method ($p = 0.002$) in 10 cell lines and in samples from 10 benign and 10 malignant tumours[299]. An additional advantage of the method is that it allows simultaneous detection of phenotypic characteristics of individual cells, such as markers of cell cycle stage or expression of surface membrane markers.

In brief, the cells that are the subject of TL analysis are mixed with reference cells that have high telomere content (1301 cells). The cells are then fixed, permeabilised and labelled with an 18mer fluorescein (FITC)-conjugated peptide nucleic acid (PNA) probe complementary to the telomere repeat sequence $(CCCTTA)_3$. They are then counterstained with propidium iodide (PI), to allow measurement of relative DNA content, thus allowing identification of the stage in the cell cycle. Telomere and DNA content measurements are then acquired by flow cytometry, and analysed (Figure 3.6). A relative telomere length (RTL) is calculated for each sample as the ratio of the peak areas of the telomere signals obtained from the test cells and the control 1301 cells, after correcting for background fluorescence and the DNA index of cells at G0/G1 (4N for 1301s cells and 2N for WIL2-NS cells or lymphocytes) (Figure 3.7).

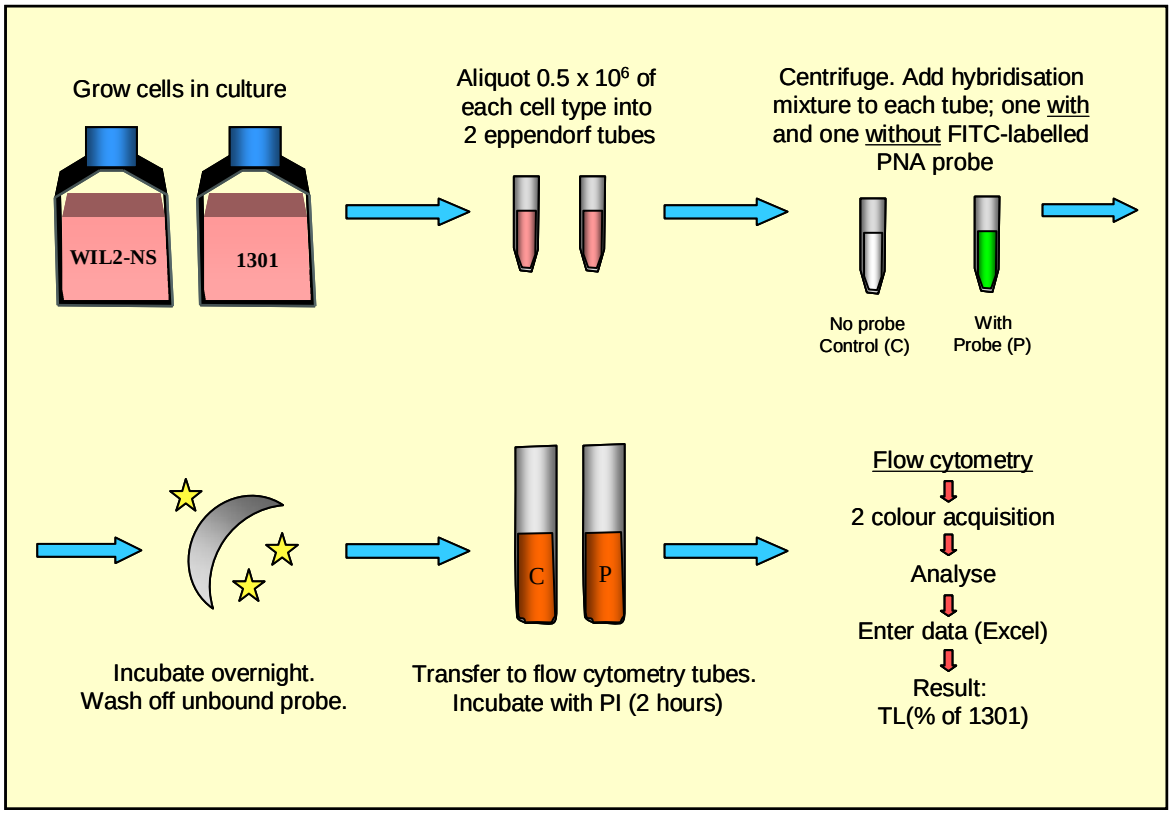

Figure 3.6 Overview of protocol for measurement telomere length by flow cytometry. Test cells and reference cells are cultured separately. Before analysis, duplicate samples were prepared by mixing 0.5 x 10^6 cells of each type, giving a total of 1 x 10^6 cells per tube. After centrifugation, the pellet in one tube was resuspended in hybridisation mixture, while the pellet in the other was resuspended in hybridisation mixture containing the FITC-conjugated PNA probe complementary to the telomere repeating sequence. Tubes were incubated overnight and the cells were then washed to remove unbound probe. Cells are then labelled with propidium iodide (PI) to allow estimation of ploidy and thus stage in the cell cycle. Fluorescence of FITC and PI was then acquired by two-colour flow cytometry. Analysis of the data allowed estimation of relative telomere length, which is expressed as the mean fluorescence of the test cells in G_O/G_1 as a percentage of the mean fluorescence of the 1301 reference cells in G_O/G_1.

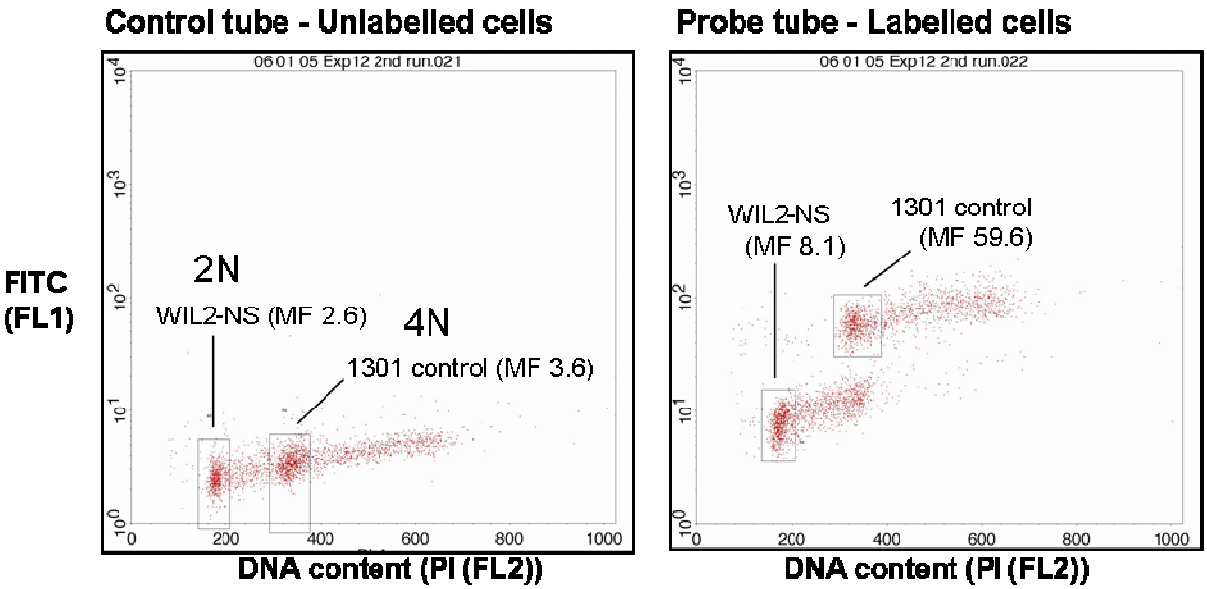

$$\text{TL (\%1301)} = \left[\frac{\text{(mean FL1 of test cells with probe) – (mean FL1 of test cells without probe) x DNA index of 1301 cells}}{\text{(mean FL1 of 1301 cells with probe) – (mean FL1 of 1301 cells without probe) x DNA index of test cells}} \right] \text{X 100}$$

In the example shown the TL of WIL2-NS relative to 1301 was calculated as follows:

$$\text{TL (\%1301)} = \left[\frac{(8.1 - 2.6) \times 4}{(59.6 - 3.6) \times 2} \right] \text{X 100} = 19.6\%$$

Figure 3.7 Estimation of relative telomere length (RTL) by flow cytometry, using paired tubes containing both test and reference (1301) cells. Cells in the unlabelled control tube are used to measure background fluorescence. Cells in the paired tube are labelled with a FITC-conjugated peptide nucleic acid (PNA) probe complementary to the telomere sequence. TL relative to that of 1301 cells is then calculated using the equation above, which incorporates correction for ploidy (DNA index) of the different cell populations, where FL1 = fluorescence detected in FL1 (green fluorescence) channel, DNA index of 1301 reference cells = 4, and DNA index of lymphocytes (test cells) = 2. The coefficient of variation (mean ± SE) of duplicate measurements was 9.4 ± 1.0%. (MF, mean fluorescence).

3.4.2 Peptide nucleic acid (PNA) probe

Peptide nucleic acid (PNA) probes are synthetic DNA oligonucleotide analogues that are capable of binding to DNA in a sequence-specific manner, obeying the Watson-Crick base pairing rules. In a PNA molecule, the sugar phosphate backbone has been replaced by a neutral peptide/polyamide backbone, keeping the distances between the bases exactly the same as in DNA[300]. PNA molecules are superior to DNA probes in terms of sensitivity and specificity. They are highly resistant to degradation by DNases, RNases, proteinases, and peptidases, and they bind with high affinity [300-303]. The PNA probe used to detect telomere sequences was purchased as Dako Kit# K5327 (Dako, Denmark). The kit, which contains a 18mer PNA oligopeptide labelled with fluorescein isothiocynate (FITC), has been used previously for estimation of TL[304].

3.4.3 1301 reference cells

The cell line (WIL2-NS) and fresh lymphocytes used in all experiments reported in this thesis are diploid (have a ploidy of 2N), whereas the 1301 reference cells are tetraploid (4N). Thus a correction for ploidy at G0/1 is required to compare TL between 2N and 4N cells, using the equation shown in Figure 3.7). To ensure consistency of TL in the reference cell line, 1301 cells were grown in large batches and aliquots were stored in liquid nitrogen until required (see Chapter 3.2).

3.4.4 Labelling of telomeres using the FITC-conjugated PNA probe

Cells were labelled, data acquired by flow cytometry, and analysed according to manufacturer's instructions for Dako Kit# K5327 (Dako, Denmark). The protocol used to label telomeres is summarised graphically at Figure 3.6. Samples of cells were removed from culture, washed twice in PBS at RT, counted (Chapter 3.2.2) and an estimate made of viability (Chapter 3.2.3). The cells were then resuspended in PBS at a concentration of 1 x 106 cells/ml. Reference cells (1301) were thawed immediately prior to use (as per Chapter 3.2.5) and resuspended in PBS at a concentration of 1 x 106 cells/ml. 500µl of sample cells and 500µl of 1301 cells were then combined in duplicate 1.5ml microcentrifuge tubes. The combined cell suspensions were then centrifuged at 500g for 5 minutes and the supernatant aspirated. The pellet in each of the paired tubes, which contained mixed sample and reference cells, was resuspended and mixed well in either (a) 300µl of hybridisation solution (containing formamide); or (b) 300µl hybridisation solution containing formamide plus the 18mer fluorescein-conjugated PNA probe complementary to the telomere sequence. The former was used to estimate the background fluorescence of the test and reference cells. The samples were then incubated at 82°C in a heating block for precisely 10 minutes to denature

DNA, followed by an overnight incubation at RT for annealing of the PNA probe. To minimise damage to cells, all vortexing steps in the manufacturer's protocol were replaced either by gentle pipetting or tapping of the tube to mix and/or resuspend cells.

Following the overnight incubation, the cells were washed in 1ml of 1 x wash buffer (provided by kit), and incubated at 40°C for 10 minutes. The samples were then centrifuged for 5 minutes at 500g and the supernatants aspirated. A second wash was performed, repeating the above steps, following which the cell pellets were resuspended in 300µl of 1x propidium iodide (PI) solution containing RNase A (provided by kit) (Note that the manufacturer's protocol includes 500µl of 1 x PI solution. However, reducing the volume to 300µl was found to be optimal for speed of acquisition, as well as allowing voltage to be set at a level which allowed the capture of fluorescence data from all events in the FL3 channel during flow cytometry). After transfer to labelled 5ml polystyrene flow cytometer tubes (Becton Dickinson, NJ, USA), the tubes were incubated at 4°C for at least two hours (but not more than 24 hours) prior to acquisition by flow cytometry. Due to the light sensitive nature of FITC, all steps of the labelling process were performed under reduced lighting conditions, and tube racks were covered by aluminium foil at all times.

3.4.5 Data acquisition by flow cytometry

Data were acquired using a FACSCalibur flow cytometer, incorporating BD CellQuestTM Pro software (v5.2) (Becton Dickinson, NJ, USA) and excitation at 488nm. The data were recorded using a logarithmic scale for FL1-H (detection of FITC-labelled probe) and a linear scale for FL3-A (detection of PI staining) as shown in Figure 3.8A. Ten thousand events were acquired per tube. Dead cells and debris were gated out using forward scatter (FSC) and side scatter (SSC) plot (Figure 3.8A). Cell aggregates were excluded by use of a plot displaying PI-A (FL3-A) and PI-W (FL3-W), where PI-A represented the area under the curve for a given event, and PI-W represents the width of the pulse. Displaying PI-W data allowed the identification, and exclusion, of events for which the pulse width exceeded that of a single cell. Accordingly, numbers of events for which fluorescence data was acquired were based only on those in the R1 region (Figure 3.8B). Voltage settings for FL1-H (FITC) remained constant throughout all experiments, while voltage for FL3-H (PI) was adjusted for each tube to ensure that all populations were clearly visible in the relevant plot. Only cells in G0/1-phase of the cell cycle were gated for analysis, because these populations were most numerous and were clustered tightly due to their precise 2N or 4N content of DNA.

3.4.6 Estimation of relative telomere content of cells

Fluorescence intensity data acquired using flow cytometry were analysed using BD CellQuestTM Pro software (v5.2). Each pair of tubes generated an estimate of telomere content relative to that of the 1301 reference cells (Figure 3.7). Because telomere content is related to the average overall length of repetitive telomere sequence within the test cells, this measurement will be referred to henceforth as "telomere length" (TL). This calculation used mean fluorescence in the FL1-H channel (FITC) from analysis of G0/G1 cells in both the labelled and the unlabelled tubes (Figure 3.7). Background fluorescence for each cell type in the control (unlabelled) tube was subtracted from the signal derived from bound probe in the paired tube labelled with FITC-PNA. The calculation of TL in the test cells relative to 1301 cells used the following equation, which incorporates correction for ploidy (DNA index) of the test and reference cells:

$$\text{Average Telomere Length (\%1301)} = \left[\frac{\text{(mean FL1 of test cells with probe) – (mean FL1 of test cells without probe) x DNA index of 1301 cells}}{\text{(mean FL1 of 1301 cells with probe) – (mean FL1 of 1301 cells without probe) x DNA index of test cells}} \right] \text{X 100}$$

where FL1 = fluorescence detected in FL1 (FITC) for the respective cells, DNA index of 1301 reference cells = 4, and DNA index of WIL2-NS or PBL (test cells) = 2 (Figure 3.7).

The average telomere fluorescence per haploid genome in the test cells is expressed as a percentage of the average telomere fluorescence per haploid genome in the reference cells (1301 cell line). Henceforth, this measurement will be referred to as telomere length (TL) for convenience. The coefficient of variation (mean ± SE) of duplicate measurements was 9.4 ± 1.0%.

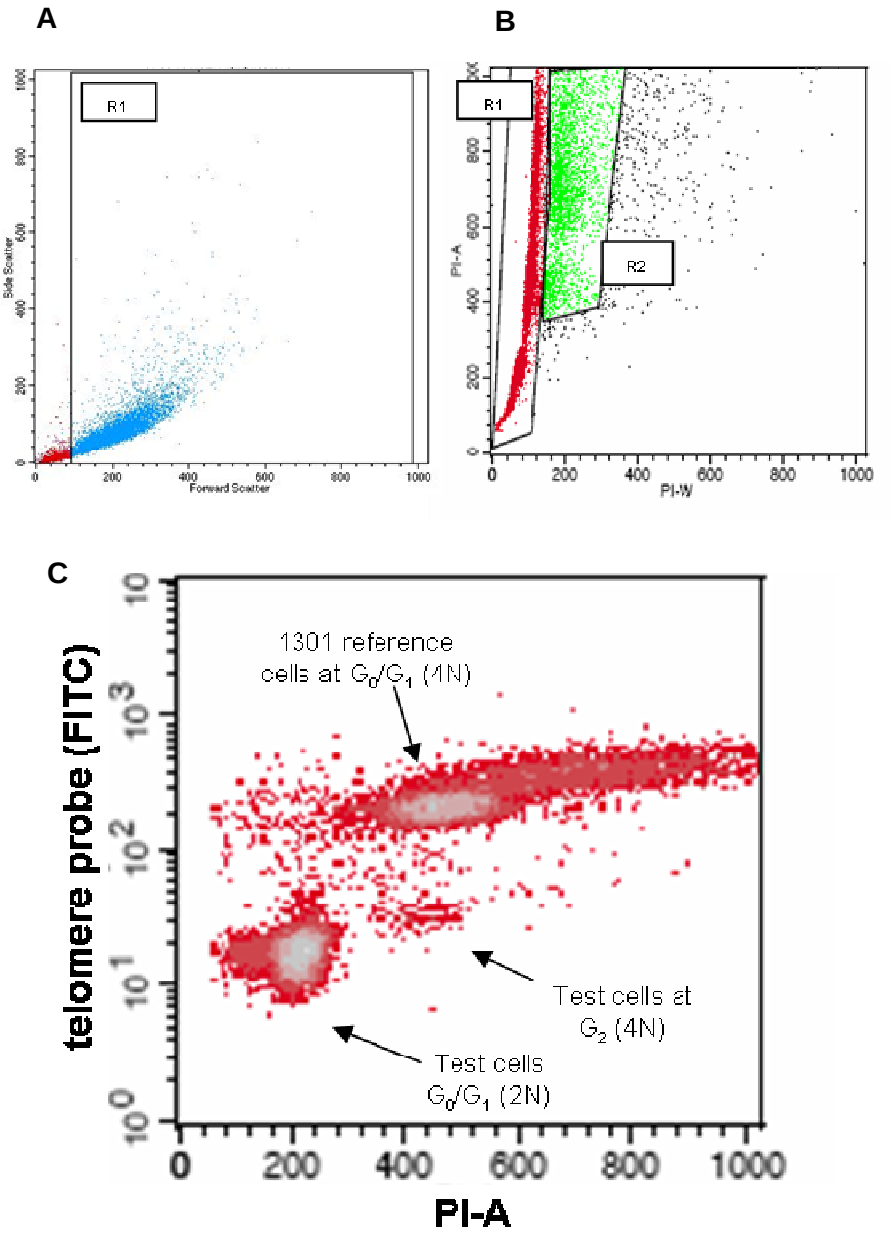

Figure 3.8 Data acquisition for analysis of telomere length, using flow cytometry

(A) Forward and side scatter plot. The y axis displays side scatter (SSC) indicating cell complexity, while the x axis displays forward scatter (FSC) indicating cell size. Only events in region 1 (R1) were included in analysis of TL and ploidy. Events outside region 1 (R1) were excluded as dead cells or debris. (B) Plot used to distinguish single cells from cell aggregates. FL3-A (PI-A), displayed on the y axis, separates events based on area under the curve. FL3-W (PI-W), displayed on the x axis, separates events based on pulse width. Events registering a larger PI-W value (aggregates of two or more cells) were gated in region 2 (R2), and excluded from analysis. Only events in region 1 (R1) were included in analysis of TL and ploidy. (C) Dot plot of fluorescence intensity of bound FITC-PNA probe and intercalated PI in a sample containing lymphocytes plus 1301 reference cells. The y axis displays fluorescence intensity of FITC (FL1-H channel), while the x axis displays fluorescence of PI (FL3-A channel). The fluorescence intensities associated with G_0/G_1 diploid (2N) and tetraploid (4N) cells are shown.

3.5 MOLECULAR BIOLOGY

3.5.1 DNA isolation

DNA was isolated using the silica-gel membrane based DNEasy blood and tissue kit (Qiagen, Cat no. 69506), following the manufacturer's instructions. The use of phenol and high temperatures (>56°C) were avoided to minimise DNA damage[305]. In brief, samples of viable lymphocytes stored either at -80°C or in liquid nitrogen were thawed and washed twice in PBS (as per Chapter 3.2.5). 20µl of proteinase K solution (1mg/ml) and 200µl of DNeasy (Qiagen) AL (lysis) buffer were added to the pellet and mixed thoroughly by vortexing. The cells were then incubated at 37°C for 2hrs. Following incubation, 200µl of ethanol was added and vortexed for 10 seconds. The mixture was transferred into a fresh microtube (spin column), housed in a collection tube, and centrifuged for 1 min at 8000rpm (Centrifuge 5415R, Eppendorf). The spin column was placed inside another collection tube and washed with 500µl of DNeasy (Qiagen) AW1 (wash) buffer by centrifugation for 1 minute at 8000rpm. The spin column was placed inside a further collection tube and washed again with 500µl DNeasy (Qiagen) AW2 (wash) buffer by centrifugation for 3 minutes at 14,000rpm to dry the DNeasy membrane. The spin column was then place in a 1.8ml microtube (Eppendorf) and DNA was eluted from it by adding 100µl of DNeasy (Qiagen) AE (elution) buffer and centrifuging at 8000rpm for 1 minute. The final step was repeated into the same collection tube using a further 100µl of AE buffer.

The concentration of DNA in a 2µl sample was estimated using a Nanodrop which provides a concentration in ng/µL (Model ND-1000, NanoDrop Technologies, Delaware, USA). Samples were stored at 4°C prior to use.

Several modifications were made to standard DNA isolation methods to increase the integrity of the purified material. Previous studies have reported that oxidative adducts can form spontaneously during the DNA isolation process and affect the integrity of the purified DNA[306,307]. To minimise *in vitro* DNA oxidation, a modified version of the protocol outlined by Lu *et al* was incorporated into the DNEasy standard protocol[305]. Immediately prior to commencing the isolation procedure, all buffers were supplemented with 50µM phenyl-tert-butyl nitrone (Sigma, Australia). The phenyl-tert-butyl nitrone acts as a free radical trap and scavenger. In addition, all solutions were purged for five minutes with nitrogen to reduce the levels of dissolved oxygen. An additional modification was introduced to reduce the formation of abasic sites in the DNA. Although the protocol for the Qiagen DNeasy kit specified

incubation at 70°C for 10 minutes, a longer incubation at a reduced temperature was employed to reduce induction of abasic sites, which are known to form at higher temperatures[305].

3.5.2 Assessment of uracil incorporation into telomeric DNA by Quantitative Real-time PCR (qPCR)

The amount of uracil present in telomeric repeat sequences was assessed using a modified quantitative Real-Time PCR (qPCR) method to measure telomere length, incorporating additional digestion steps. This method was conceived and developed by Prof Michael Fenech and Dr. Nathan O'Callaghan in this laboratory. At the time of writing this method had not yet been fully refined and validated. In brief isolated sample DNA is digested with uracil glycosylase to generate abasic sites where uracil was present, leaving the phosphodiester backbone intact. Telomeric repeat sequences are then amplified by qPCR. When an abasic site is encountered, the DNA polymerase will either pause or stop completely, resulting in a reduction in amplification efficiency. These sequences are observed as higher Cq values than in those of the undigested telomere sequence (Figure 3.9A). The difference in Cq values generated by samples that have, and those that have not, been digested with uracil glycosylase is then used to calculate the amount of uracil present in the telomeric DNA, using a standard curve (Figure 3.9B).

3.5.2.1 DNA digestion with uracil glycosylase

The concentration of isolated DNA for each sample was quantified using a spectro-photometer (Model ND-1000, NanoDrop Technologies, Delaware, USA). The DNA digestion was performed as follows: a total of 300ng of DNA was used with 1unit of uracil glycosylase (UDG) (New England Bioloabs) and appropriate buffer. Water was added to each well to achieve a final volume of 30µL. An undigested sample (for each DNA sample) was also prepared and treated in the same way. All preparatory steps involving uracil glycosylase were performed on ice to maintain the enzyme in an inactive state until required. Digestion was instigated by incubating the plates at 37°C for precisely 3 hours, followed by a 5' incubation at 80°C to denature the enzyme and halt the reaction. Digestion plates were then cooled to RT and stored at 4°C prior to use.

3.5.2.2 Amplification of telomeric DNA in digested and undigested samples

Telomeric DNA sequences in the digested and undigested samples were amplified using a modified form of the qPCR method for absolute telomere length, as described by O'Callaghan *et al* (2008)[308]. Each 20µl reaction was performed in duplicate as follows: 50ng DNA, 1 x SYBR Green master mix, 100nM telo1 forward primer (CGGTTTGTTTGGGTTTGGGTTT

GGGTTTGGGTTTGGTT), 100nM telo2 reverse primer (GGCTTGCCTTACCCTTACCCTT ACCCTTACCCTTACCCT)[308,309], and 3µl water to make the final volume in each well consistent at 20µl. Cycling conditions were: 10min at 95°C, followed by 40 cycles of 95°C for 15sec, 60°C for 1 min. All samples were run on an Applied Biosystems (AB) 7300 Real Time PCR System and ABI 7300 Sequence Detection system with the SDS Ver. 1.9 software (Applied Biosystems, Foster City, CA).

3.5.2.3 Analysis of uracil content in telomeric DNA

A standard curve was established by substitution of known frequencies of uracil bases into a synthesised 84-mer oligonucleotide containing 14 TTAGGG repeats. Assays were performed using the modified oligonucleotides to determine a standard curve for numbers of uracil bases present per kilobase of telomeric sequence (Figure 3.9B). The resulting standard curve had a correlation coefficient (R^2) of 0.9967.

After amplification of sample DNA was complete, the AB software provided a Cq value for each reaction which was exported into MS Excel where the final calculations were performed to determine the number of uracil bases per kilobase of telomeric DNA. The following equation was used:

$$y = \Delta Cq \quad (Cq_{dig} - Cq_{undig})$$

$$x = \frac{(\log_{10} y + 1.2694)}{0.0256}$$

where x = the number of uracil bases per kb of telomeric DNA; Cq_{dig} = Cq value of the digested sample well, and Cq_{undig} = Cq value for the corresponding undigested well for the same sample. The values 0.0256 and 1.2694 were obtained from the slope and y intercept, respectively, of the equation for the standard curve. The mean result for day 0 was then set as 100%, and each sample calculated as a percentage relative to this value.

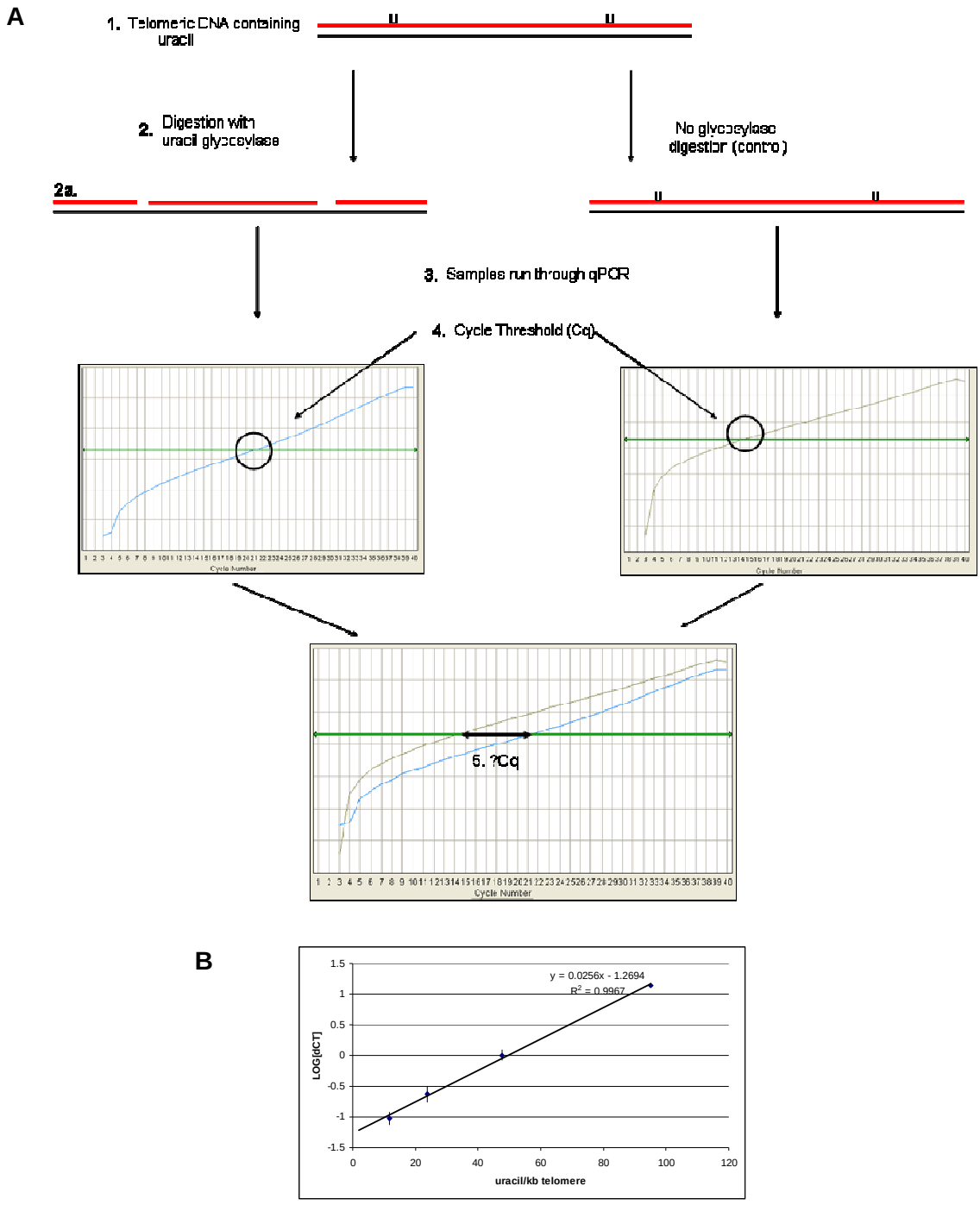

Figure 3.9 qPCR Assay for detection of uracil in telomeric DNA sequences. (A) (1) Uracil incorporated into telomeric DNA; (2) Isolated DNA samples are paired; one sample is digested with uracil glycosylase, the other remains undigested (control). (2a) Uracil glycosylase excises aberrant uracil leaving abasic sites (3). Samples are analysed by qPCR. (4) Upon encountering an abasic site the DNA polymerase pauses, resulting in a lower Cq value due to slower amplification, compared with the undigested sample (5). (B) Standard curve established by substitution of known frequencies of uracil bases into a synthesised 84-mer oligonucleotide containing 14 TTAGGG repeats. The equation of the line was used to calculate uracil bases present in telomeric sequence.

3.5.3 LINE1 assay for determining global hypomethylation

3.5.3.1 Overview

Global methylation was quantified using the LINE1 USP quantitative real-time PCR (qPCR) method. The LINE1 assay for data presented in this thesis was conducted by Dr. Varinderpal Dhillon, Ms. Susan Mitchell and Ms. Thu Ho at the CSIRO laboratories in North Ryde, NSW. Their data is presented as part of this thesis, with due acknowledgement. All data analyses were conducted by the author.

DNA methylation occurs by the addition of a methyl group to the fifth carbon position of the pyrimidine ring in cytosine bases, via a methyltransferase enzyme[310]. This epigenetic modification is a mechanism that is employed by cells to control gene transcription, and it occurs at approximately 80% of 5'-CpG-3' dinucleotides (CpG island)[310]. LINE1 sequences are repeated numerous times throughout the genome and are normally heavily methylated. Accordingly, measurement of the degree of methylation of these sequences can be used as a representative indicator of global DNA methylation.

Long and short interspersed elements (LINE and SINE respectively) are retrotransposons constituting approximately 33% of the human genome[311]. These are repeating sequences that are transcribed to RNA, then converted back to DNA by a reverse transcriptase, prior to integration into the genome[311]. Long interspersed nuclear elements (LINEs) are predominantly represented by LINE1[311]. Intact LINE1 elements are approximately 6kb in length, with approximately one million copies present in the human genome. In somatic cells a significant proportion of LINE1 sequences are silenced by high levels of cytosine methylation at the 5' position on the pyrimidine ring[311]. Due to the high level of cytosine methylation that occurs consistently in these sequences, and the high frequency throughout the genome, LINE1 represents an ideal target for assessing alterations in methylation of the genome as a whole.

In brief, the assay is conducted on isolated DNA pre-treated with sodium bisulphite to convert unmethylated cytosine residues to uracil. In subsequent amplification cycles uracil will then be replaced by thymine which will, in turn, base pair with adenosine. As such, the ratio of methylated and unmethylated cytosine residues in the original DNA sample can be calculated. Sample DNA is amplified in the presence of primers specific to the LINE1 sequence. DNA concentrations for each sample are normalised by quantifying ribosomal DNA in each well.

3.5.3.2 Sodium bisulphite pre-treatment

Isolated DNA is pre-treated using the protocol provided for the kit *EZ DNA Methylation-Gold Kit™* (Zymo Research, USA). This pre-treatment exploits the different sensitivities of cytosine and 5-methylcytosine (5-MeC) to deamination by bisulphite under acidic conditions, with cytosine residues being converted to uracil, while 5-MeC remains intact[312]. Briefly, 1µg DNA is modified using CT Conversion Reagent (Zymo Research, USA) and samples were incubated at 98°C for 10 minutes, 64°C for 2.5 hours and 4°C for 30 minutes. DNA samples were desalted through Zymo-Spin IC columns (Zymo Research) and desulphonated using M-Desulphonation buffer (Zymo Research) at RT for 15 minutes. Following two washes with M-Wash buffer (Zymo Research), DNA was eluted using M-Elution buffer (Zymo Research). Modified DNA was stored immediately at -20ºC.

3.5.3.3 Standard curve preparation

Human genomic DNA (Roche, Australia) was amplified using Repli-G mini kit (Qiagen). This DNA is 100% unmethylated and is termed genomified DNA. Serial dilutions of this unmethylated DNA, using fully methylated DNA as a diluent (Chemicon, USA) were prepared as follows to generate a standard curve: 100% unmethylated, 25% unmethylated + 75% fully methylated, 12.5% unmethylated + 87.5% fully methylated, 6.25% unmethylated + 93.7% fully methylated, 3.125% unmethylated + 96.875% fully methylated, 1.563% unmethylated + 98.438% fully methylated and 100%.

3.5.3.4 Normalisation of samples using ribosomal DNA qPCR

Concentrations of bisulphite treated DNA were verified using ribosomal DNA (rDNA) qPCR. Each 20µl reaction was performed in duplicate, in a 96-well plate, containing 10ng pre-treated DNA, 10X Platinum® Taq buffer without Mg^{2+}, 200uM deoxynucleotide triphosphate (dNTP) mix (2mM each), 50mM $MgCl_2$, SYBR green 1 (100X), Platinum® Taq enzyme (5U/ml), 5µM forward primer (5' – CCTCTTCCTCCGTGGGTGGAG TTATTGTTTT – 3'), 5µM reverse primer (5' – GGAGG CAAATAAAATTTCCACCT – 3'), and water. The reaction was run on BioRad Icycler (Biorad) using the following cycling conditions: 95°C for 2 minutes (min), 5 cycles of 95°C for 15 seconds (sec), 50°C for 40sec, 72°C for 20sec, followed by 45 cycles of 95°C for 15sec, 60°C for 40sec and 72°C for 20sec. Dilution for all samples were then adjusted to match that of the 100% methylated commercial sample.

3.5.3.5 LINE 1 Assay

qPCR for LINE 1 assay was applied for all samples and standards. Primer mix was prepared containing 1µl (100pmol) forward USP primer (5'- TAGTGTGTGTGTGTATTGTGT GTGAGTT-3') and 1µl (100pmol) reverse primer (5'– ACCCAATTTTCCAAATA CATCCA–3') and 98µl water. Master mix was then prepared, containing 10X Platinum® Taq buffer without Mg^{2+}, primer mix, SYBR green 1 (100X), dNTP-mix (2mM of each), $MgCl_2$ (50mM), Platinum® Taq enzyme (5U/ml) and water. Each 20µl reaction was performed in triplicate, in a 96-well plate, with 10ng (2µl) of bisulphite treated DNA and 18µl SYBR Green Master mix. The plate was then centrifuged at 3000rpm for 3 min. The reaction was run on BioRad Icycler (Biorad) using the following cycling conditions: 95°C for 2 minutes, followed by 50 cycles of 95°C for 20 seconds, 62°C for 20 seconds and 72°C for 20 seconds.

qPCR for rDNA was run again on all samples and standards using the protocol detailed above in 3.5.3.4. Each reaction was conducted in triplicate. The rDNA Cq values generated were used to correct for the amount of DNA in each LINE 1 sample.

3.5.3.6 Calculation of hypomethylation DNA relative to Day 0

The calculation for the percentage of unmethylated DNA in the original sample is based on the mathematical model proposed by Pfaffl[313]. Efficiencies (E) for LINE 1 and rDNA qPCR reactions are calculated from the standard curve for each, using the equation: $E = 10^{-1/slope}$. Hypomethylation was then calculated using the following equation:

$$\text{Ratio} = \frac{[E_{target}]^{\Delta Cq\ target\ (Cq\ (std) - Cq\ (sample))}}{[E_{ref}]^{\Delta Cq\ ref\ (Cq\ (std) - Cq\ (sample))}}$$

Where E_{target} = Efficiency of LINE 1 qPCR

And E_{ref} = Efficiency of ribosomal DNA (reference) qPCR

Cq std = mean Cq of unmethylated standards using rDNA qPCR. For these calculations, based on prior experience of the operators, the Cq value for the 5% methylated standard was selected, and for the reference the Cq value for 100% methylated standard was selected. The ratio obtained from this equation was then converted to a value relative to 1.0, where 1.0 was the degree of hypomethylation of the Day 0 sample. This value was the mean hypomethylation ratio for Day 0 samples. Values for all other samples were divided by the mean Day 0 value to obtain a relative value. It is this data that is presented in this thesis.

3.5.4 Allelic discrimination: MTHFR and MTR

Isolated DNA was genotyped for *MTHFR C677T* and *MTR A2756G* polymorphisms using Applied Biosystems (ABI) Assays-on-Demand (MTHFR C677T 1202883 and MTR A2756G 12005959) and TaqMan® Universal PCR Master mix, without AmpErase® UNG. Approximately 20ng of genomic DNA was used per 20.0µl reaction. PCR amplification was conducted using an Applied Biosystems 7900 Real Time PCR System and genotypes were identified using an ABI 7300 Sequence Detection System with the SDS Ver. 1.9 software (Applied Biosystems, Foster City, CA). Each reaction was performed in duplicate.

Hydrolysis probes were used for allelic discrimination to determine genotype. The presence of two primers encompassing the polymorphism, as well as a specific probe for each allele, within a single reaction allows the detection of the two possible variants within the target template sequence. Each DNA probe is complementary to the sequence of one allele of the polymorphism and is labelled with a different fluorescent reporter dye, such as FAM or VIC; the reporter dye then represents a specific polymorphism within each sample. The reaction involves four main components; forward and reverse primers which bind either side of the polymorphism of interest, a DNA polymerase which extends the primers and which also contains a 5'-3' exonuclease activity, and the DNA probes. Each probe has one base altered to provide binding specificity for the single nucleotide polymorphism (SNP) being tested, a fluorophore (reporter dye; FAM or VIC) and a fluorophore quencher. When the probe is intact the fluorescent signal of the reporter dye remains silenced. Following binding to the target sequence, however, the reporter dye and the quencher become dissociated due to the exonuclease action of the DNA polymerase during strand replacement and primer extension. Dissociation results in a reduction of the quenching effect, thus allowing the reporter dye to fluoresce; it is this signal which can be recorded and quantified to determine the genotype of a sample. Increases in the fluorescence of reporter molecule containing FAM or VIC indicate specific allele homozygosity, while an increase in both signals indicates allele heterozygosity (Figure 3.10).

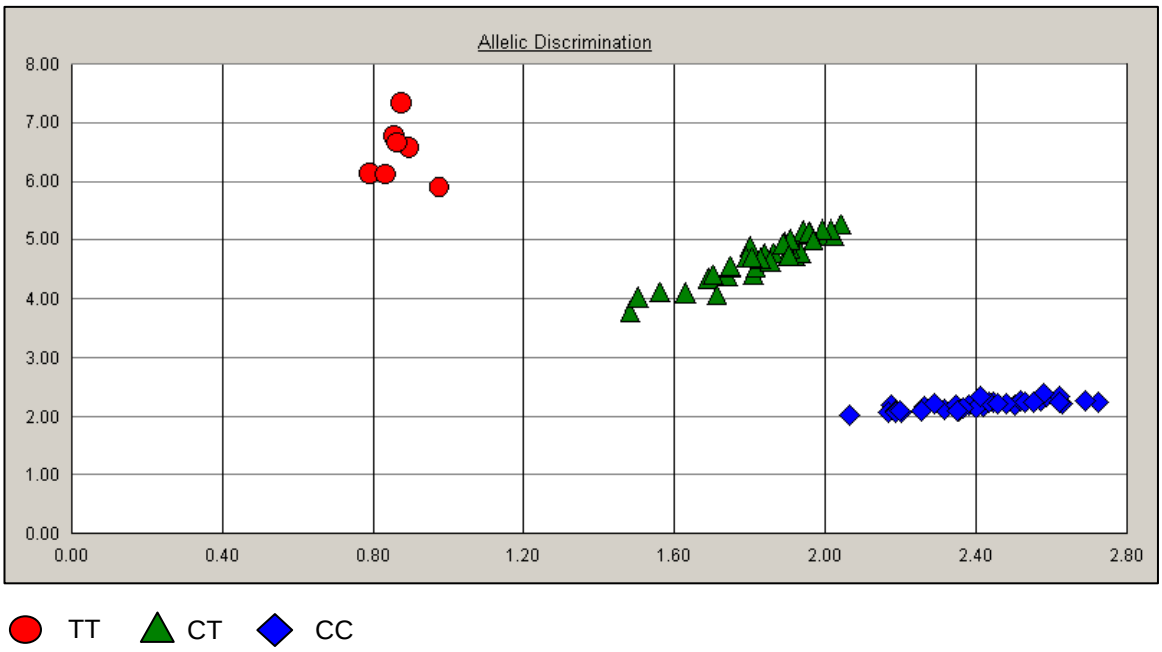

Figure 3.10 Allelic discrimination scatter plot for allele X (T) versus allele Y (C) for methylene tetrahydrofolate reductase (*MTHFR*) *C677T*.

3.5.5 Analysis of gene expression

3.5.5.1 Isolation of RNA from WIL2-NS cells

RNA was isolated from fresh WIL2-NS cells during experiments testing the effects of short and long term exposure to various concentrations of FA. This procedure was performed by Dr. Nathan O'Callaghan at CSIRO Food & Nutritional Sciences. Total RNA was extracted from the cells using TRIzol (Ambion), as per the manufacturer's directions. A 0.5mL volume of TRIzol was used to homogenise each sample. The only alteration from the manufacturer's directions was the use of 2µg/mL glycogen (Ambion) and 5mM sodium acetate to aid RNA precipitation.

3.5.5.2 cDNA Synthesis from Isolated RNA

RNA samples were thawed slowly on ice prior to measurement of concentration using a spectrophotometer (Model ND-1000, NanoDrop Technologies, Delaware, USA). *SuperScript™ III First-Strand Synthesis system for RT-PCR* (Invitrogen, Cat No 180800-051) was used to create cDNA from purified RNA, using a modified viral reverse transcriptase enzyme (*SuperScript™ III)*. 5µg of DNA was then incubated with random hexamer primers, according to manufacturer's instructions. Each sample was transcribed into cDNA in duplicate. The mixture was treated at 65°C for 10 minutes (PCR, Corbett Research) to denature any double strands and to dissociate any bound proteins. Vials were then placed immediately on ice for at least 1 minute. 10µl of synthesis mix was then added containing buffer, 25mM $MgCl_2$, 0.1M dithiothreitol (DTT), RNAseOUT (RNAse inhibitor) and the polymerase *Superscript III RT*. Vials were then returned to the PCR for 10 minutes at 25°C for the annealing step. The cDNA synthesis reaction was carried out at 50°C for 50 minutes, followed by a 5 minute heating step to 85°C to inactivate the polymerase and stop the reaction. Samples were then stored at 4°C until required. All steps were performed using surfaces, gloves and equipment that had been cleaned with RNAse Zap. Samples were stored at -20°C until required.

3.5.5.3 Measurement of hTERT Gene Expression by qPCR

Telomerase (*TERT)* expression was measured by hydrolysis probe assay from Applied Biosystems (Catalogue #HS00162669). Reactions were multiplexed to examine both reference and target mRNA expression levels from a single tube. Gene expression was normalised with respect to the reference gene *GAPDH* (Applied Biosystems, catalogue #4333764F). All samples were run in duplicate with cDNA, Taqman mastermix, *GAPDH* mix (forward and reverse primers conjugated to fluorophore "VIC"), *TERT*mix (forward and

reverse primers conjugated to fluorophore "FAM") and water to make the volume up to 20µl per well. "No template control" wells were also run using 2µl water instead of cDNA.

All samples were run on an Applied Biosystems 7300 Real Time PCR System and ABI 7300 Sequence Detection system with the SDS Ver. 1.9 software (Applied Biosystems, Foster City, CA). Cycling conditions were: 10min at 95°C, followed by 40 cycles of 95°C for 15sec, 60°C for 1 min.

The level of expression of a specific gene in each sample was quantified by measuring the level of fluorescence relative to that of day 0 samples. Relative gene expression was calculated using the comparative ΔΔCq method, where day 0 samples were used as the comparator; *ie.* ΔCq values of day 0 samples were averaged and set as 1.0 for comparative expression determination. The relative expression value is shown as $2^{-\Delta\Delta Cq}$ where –ΔΔCq was calculated by the difference of ΔCq between experimental and comparator.

3.6 MICRONUTRIENT ANALYSES IN EXPERIMENTAL MEDIUM AND BLOOD SAMPLES

Folate concentration was measured in medium prepared prior to the commencement of each *in vitro* study (see Chapters 3.2.1.1 and 3.2.1.2), and also in plasma and red blood cell samples taken from human volunteers. L-homocysteine (Hcy) concentrations were measured in spent medium from *in vitro* studies, and in plasma from volunteer samples. Plasma vitamin B12 (B12) was measured in human plasma samples. These measurements were performed in the certified routine diagnostic laboratory of the Department of Chemical Pathology, Institute of Medical and Veterinary Sciences (IMVS), Adelaide, South Australia. The coefficient of variation of duplicate measurements did not exceed 5%.

All blood samples were taken following an overnight fast, and written consent was provided by volunteers. Samples were collected in 9ml Lithium-Heparin tubes, held immediately on ice, and processed within 2 hours of collection. Samples were centrifuged for 20 minutes at 410g to separate plasma from the cell fraction. 2ml aliquots from each sample of plasma, were provided to the certified routine diagnostic laboratory of the Department of Chemical Pathology, Institute of Medical and Veterinary Sciences (IMVS) for Hcy, folate and B12 assays.

3.6.1 Measurement of L-homocysteine in spent medium and plasma

The concentration of Hcy was measured in spent medium from *in vitro* studies as well as in plasma prepared from samples of venous blood. Aliquots of 2ml of spent medium, or fresh plasma, were stored frozen at -20°C prior to Hcy quantification. The concentration of Hcy in samples was expressed as µmol/L. The IMVS reference range for (fasted) plasma samples was 4.0 – 14.0 µmol/L.

Levels of Hcy were measured using the ARCHITECT® Homocysteine assay (Abbott Laboratories, IL, USA). This is a chemiluminescent microparticular immunoassay (CMIA), on the ARCHITECT® *i* system. The ARCHITECT® Homocysteine assay exhibits total imprecision of <10% within the calibration range (0.0 – 50.0 µmol/L). The analytical sensitivity of the assay is ≤ 1.0µmol/L. A calibration curve was generated prior to assay of the samples. Subsequently, every 24 hours, a single sample of all control levels was tested to ensure that the control values were within the concentration range as specified by the manufacturer. The assay was recalibrated when control(s) were out of this range, or when a new reagent kit with a new lot number was used.

In brief, the assay is a one-step procedure for the quantitative determination of total L-homocysteine. Bound or dimerised Hcy (oxidised form) is reduced by dithiothreitol (DTT) to free Hcy, which is then converted to S-adenosyl homocysteine (SAH) by the action of the recombinant enzme S-adenosyl homocysteine hydrolase (rSAHHase) in the presence of excess adenosine. The SAH then competes with acridinium-labelled S-adenosyl cysteine for particle-bound monoclonal antibody. Following a wash stage and magnetic separation, pre-trigger and trigger solutions are added to the reaction mixture and the resulting chemiluminescence is measured as relative light units (RLUs). An indirect relationship exists between the amount of Hcy in the sample and the RLUs detected by the ARCHITECT® *i* system optics[314].

3.6.2 Measurement of folic acid in fresh medium, plasma and red blood cells

Folate levels were measured in freshly prepared medium to confirm that concentrations were correct prior to commencement of *in vitro* experiments (see Chapters 3.2.1.1 and 3.2.1.2). The assay was optimised to detect FA concentrations within the range of 5 – 45nmol/L. Accordingly, medium prepared at 20nM or 30nM FA was analysed undiluted, medium prepared at 60nM FA was diluted 1:3 with water, medium prepared at 180nM was diluted 1:6, medium prepared at 300nM was diluted 1:10, and medium prepared at 3000nM was diluted 1:100 prior to analysis.

Folate concentrations were also measured in plasma and red blood cells. 2ml of plasma was provided for plasma folate analysis. 2ml whole blood was provided for red cell folate (RCF) analysis. The concentration of folate in all samples was expressed as nmol/L. The IMVS reference range for (fasted) plasma samples was 5.0 – 45.0 nmol/L. The reference range for (fasted) RCF samples was 180-900 nmol/L.

The method used for all folate measurements was the ARCHITECT® folate assay (Abbott Laboratories, Abbott Park, IL, USA), a chemiluminescent microparticular folate binding protein assay, on the ARCHITECT® *i* System. The ARCHITECT® folate assay has a total imprecision of <10% within the calibration range (0.00 – 20.0ng/mL). The analytical sensitivity of the assay is ≤0.8ng/mL. A calibration curve was generated for the ARCHITECT® folate assay prior to analysis of the samples. Subsequently, every 24 hours, a single sample of all control levels was tested to ensure that the control values were within the concentration range as specified by the manufacturer. The assay was recalibrated when control(s) were out of this range or when a new reagent kit with a new lot number was used. To convert RBC-bound folate to measurable folate, a lysis pre-treatment was performed. Two pre-treatment steps mediate the release of folate from endogenous folate binding protein. First, plasma/medium/RBC and a pre-treatment reagent (dithiothreitol (DTT) in acetic acid buffer with EDTA) were dispensed into a reaction vessel. Secondly, an aliquot of the pre-treatment solution and potassium hydroxide were dispensed into a second reaction vessel. Subsequently, an aliquot of the second pre-treatment solution was mixed with a TRIS buffer containing protein stabilisers (human albumin) and monoclonal mouse anti-folate binding protein antibody coupled to microparticles affinity bound with bovine folate binding protein (FBP). Any folate present in the sample is bound by the FBP-coated microparticles. After washing with PBS, pteroic acid-acridinium labelled conjugate (in MES buffer with porcine protein stabiliser) was added, which binds to unoccupied sites on the FBP-coated microparticles. Pre-trigger (1.32% w/v hydrogen peroxide) and trigger (0.35N sodium hydroxide) solutions were then added, resulting in a chemiluminescent reaction measurable in relative light units (RLUs). An inverse relationship exists between the amount of folate in the sample and the RLUs detected by the ARCHITECT® *i* optical system[315].

3.6.3 Quantification of Vitamin B_{12} in plasma

Plasma vitamin B12 concentration was measured studying plasma samples. 1.5ml aliquots of plasma were prepared for vitamin B_{12} quantification analysis. The concentration of vitamin B_{12} in all samples was expressed as pmol/L. The IMVS reference range for (fasted) plasma samples was 100-700 pmol/L.

Vitamin B_{12} quantification was performed using the ARCHITECT® B_{12} assay (Abbott Laboratories, IL, USA), a chemiluminescent microparticular immunoassay (CMIA), on the ARCHITECT® *i* system. The ARCHITECT® B_{12} assay exhibits total imprecision of <10% within the calibration range (0 – 2000 pg/mL). The analytical sensitivity of the assay is ≤ 39 pg/mL. Prior to quantification of the plasma samples the ARCHITECT® vitamin- B_{12} assay was calibrated using the test calibrators supplied by the manufacturer and a calibration curve was generated. Subsequently, every 24 hours, a single sample of all control levels was tested to ensure the control values were within the concentration range as specified by the manufacturer. The assay was recalibrated when control(s) were out of range or when a new reagent kit with a new lot number was used. Each sample was combined with three separate pre-treatment solutions containing (1) sodium hydroxide and potassium cyanide; (2) alpha monothioglycerol; and (3) cobinamide dicyanide in borate buffer with protein (avian) stabilisers. The pre-treated sample is then combined with diluent, and intrinsic factor (porcine) coated paramagnetic microparticles. B_{12} present in the sample binds to the coated microparticles. After washing, B_{12} acridinium-labelled conjugate is added, followed by "pre-trigger" (1.32% w/v hydrogen peroxide) and "trigger" (0.35N sodium hydroxide) solutions. The resulting chemiluminescent reaction is measured as relative light units (RLUs). An inverse relationship exists between the amount of B_{12} in the sample and the RLUs detected by the ARCHITECT *i* optical system[316].

3.7 STATISTIC ANALYSES

3.7.1 Power analysis

The primary outcome measure for the experiments presented in this thesis was telomere length. (TL) Accordingly, the experiments were designed to detect differences in this parameter. Findings in previous studies *in vivo* have shown that loss of TL proceeds at an approximate rate of 9-10% per decade[128]. Accordingly, detection of a change in TL of at least 10% was deemed to be an appropriate objective for *in vitro* studies, approximating to an ageing effect equivalent to 10 years *in vivo*. To determine the number of samples per treatment per time

point required to detect such a change at $p < 0.05$ and 80% power, a pilot experiment was conducted to measure the standard deviation (SD) of TL of WIL2-NS cells cultured *in vitro* in replete medium for 1 week and 11 weeks (n = 5 samples per group). The cells cultured for 1 week had a mean TL of 13.81, a SD of 1.2 and coefficient of variation of 8.71%. The cells cultured for 11 weeks had a mean TL of 12.69, a SD of 1.3 and a coefficient of variation of 10.35. A 10% loss in TL in the younger population would equate to a reduction in mean TL of 1.38. Using the SD values at 1 week and 11 weeks, it was calculated that 10 replicates would be needed to detect a difference of 1.39 at $p < 0.05$ and 80% power.

3.7.2 Statistic analyses

Parametric statistical analyses were used, as all variables reported here were normally distributed. Comparisons between two groups were performed using the non-paired Students t-test (published by Dr Students). One-way ANOVA was used to determine the significance of differences in a single parameter between three or more groups. Two-way ANOVA was used to determine the significance of differences between two different data sets. Pair-wise comparison of significance was determined using Tukey's test (for one-way ANOVA) or Bonferroni post test (with two-way ANOVA).

The area under the curve (AUC) for the relationship between changes in biomarkers with time, under varying treatment conditions, was also measured to obtain a total effect measure during the treatment period. In mathematical terms the AUC is the integral of the biomarker measurement from the beginning to the end of the treatment period when measurements were done. Area under the curve (AUC) data represents the net area of the region in the *xy* plane bounded by the graph, where *x* is time (days) and *y* represents the parameter in question (e.g. telomere length) (Figure 3.11 below).

ANOVA analysis, t-test, area under the curve and Pearson correlation coefficient values were calculated using Graphpad PRISM 4.0 (GraphPad inc., San Diego, CA) and SPSS for Windows 16.0 (SPSS, Chicago, IL). Multi-variate regression was used to explore age and gender adjusted data using CSS Statistica (Tulsa, Oklahoma).

The level of statistical significance was set at $p < 0.05$.

3.7.3 Area under the curve abbreviations

For the purpose of simplifying the text and figures, the following abbreviations have been used throughout this thesis:

'AUC TL'; Area under the curve for telomere length with time (days)

'AUC MNi' / 'AUC NPB' / 'AUC NBud'; Area under the curve for the total number of MNi (or NPB or NBuds) per 1000 binucleated (BN) cells, with time (days). 'AUC NPB' represents NPB scored using the standard CBMN Cyt assay scoring criteria. (In Chapters 6 and 7 the data are for 500 BN cells).

'AUC total NPB'; Area under the curve for the total number of NPB per 500 BN cells with time. This data includes BN cells displaying 'chewing-gum' morphology which were scored as containing '5' NPBs.

'AUC total DNA damage'; Area under the curve for the total number of DNA damage biomarkers scored for the CBMN Cyt assay, per 1000 BN cells, with time (days). This data includes all MNi, all NPBs and all NBuds scored within 500 BN cells, including those in cells with multiple DNA damage events, scored using the standard criteria.

'AUC LINE1 hypomethylation'; Area under the curve for LINE1 hypomethylation with time (days). (will delete if methylation data doesn't come in time)

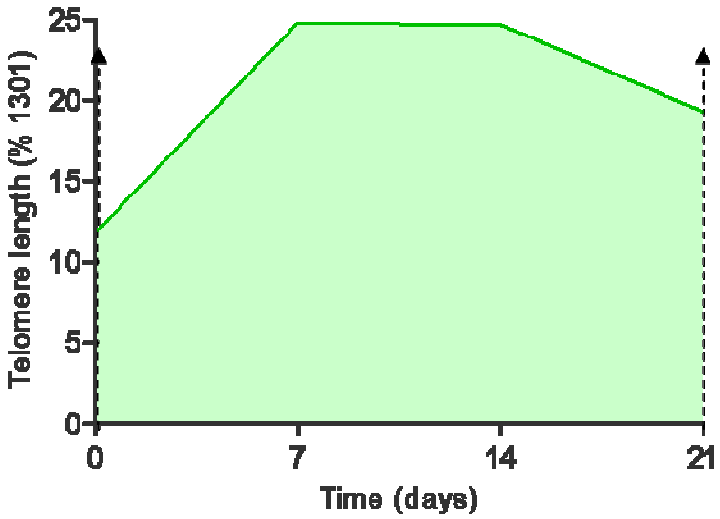

Figure 3.11 Representative example of area under the curve. Area under the curve (AUC) data presented in this thesis represents the net area of the region in the *xy* plane bounded by the graph, where *x* is time (21 days) and *y* represents the parameter in question, which, in this example is telomere length (TL).